



Norwegian University of  
Science and Technology

# Optimizing separator pressure in a multistage crude oil production plant

Øyvind Widerøe Kylling

Master of Science in Engineering Cybernetics

Submission date: June 2009

Supervisor: Jan Tommy Gravdahl, ITK



# Problem Description

This project is related to offshore oil and gas production. Oil and gas production is a complex process where many components are closely coupled and dependent on each other. With a traditional control structure the separator pressure is fixed and it is possible that an adaptive separator pressure will increase profit. The main objective of this project is to derive a steady state simulation model for a multistage crude oil production plant and optimize the separator pressure. This will be achieved through the following subgoals:

1. Explain the potential benefits of using adaptive separator pressure
2. Literature study on separator modelling. Give a presentation of different methods found in the literature and implement the method best suited for this problem.
3. Optimize the separator pressure for a multistage crude oil production plant without compressors.
4. Literature study on compressor modelling. Give a presentation of different methods found in the literature and implement the method best suited for this problem.
5. Optimize the separator pressure for a multistage crude oil production plant with gas compression.

Assignment given: 12. January 2009  
Supervisor: Jan Tommy Gravdahl, ITK



## Abstract

This thesis contains a steady state simulation model of a multistage crude oil production plant. The unstable reservoir fluid is separated into crude oil and gas in a three stage gas oil separation plant. Peng Robinson Equation of State and successive substitution is used to model the separators. The liquid output for the third stage separators is stable crude oil and the crude oil is sold on the international market.

The gas liberated in the separators is compressed by centrifugal compressors and injected into the reservoir. Several methods for modelling centrifugal compressors are discussed. The discussion concludes that Dimensionless Parameters is the best suited method for this case and this method is therefore used.

The plant studied has three separation stages at decreasing pressure and the standard control method is to use fixed separator pressure. This is not optimal and brute force optimization is used to find the optimal pressure set-points. Adaptive pressure set-points will improve product separation and therefore increase the profit. The profit is calculated as the income from crude oil sale minus the energy cost.

Using this new method, the optimum separator pressures for Snorre A are determined. As a result, the profit is increased with 0.17, 0.11 and 0.07 percent for three different inlet conditions. For one year this small increase in profit gives an extra two million dollars in income. The adaptive pressure set-points give an extension of the plant's maximum capacity for a reservoir fluid with a high gas oil ratio.



## **Preface and acknowledgments**

This thesis concludes my Master of Science degree at the Norwegian University of Science and Technology. The scope of this work is one semester and the thesis is written in the spring of 2009.

This project report has been written in collaboration with Siemens Oil & Gas Offshore AS. I would like to thank Dr. Ing Fredrik Dessen and the rest of the department. They have always answered my questions and have arranged access to the database system and a work station at Siemens.

I would like to express my sincere gratitude to my supervisor Jan Tommy Gravdahl. Gravdahl has helped me working on the right subjects and pointed out details that I have missed.

Øyvind Widerøe Kylling

June 2009, Trondheim Norway





# Contents

<b>ABSTRACT</b> .....	<b>I</b>
<b>PREFACE AND ACKNOWLEDGMENTS</b> .....	<b>III</b>
<b>1 INTRODUCTION</b> .....	<b>1</b>
1.1 PLACEMENT IN THE OVERALL CONTROL STRUCTURE .....	2
1.2 CONTRIBUTIONS OF THIS THESIS .....	2
<b>2 GAS OIL SEPARATION PLANT</b> .....	<b>3</b>
2.1 OPTIMUM PRESSURE FOR GAS-OIL SEPARATORS .....	5
2.1.1 <i>Empirical method</i> .....	6
<b>3 CHEMICAL PROCESS SIMULATOR</b> .....	<b>7</b>
<b>4 SEPARATOR MODELLING</b> .....	<b>9</b>
4.1 OPTIMIZATION ALGORITHM .....	9
4.1.1 <i>Indirect minimization</i> .....	9
4.1.2 <i>Local direct minimization</i> .....	10
4.1.3 <i>Global direct minimization</i> .....	10
4.2 THERMODYNAMIC MODELS.....	11
4.3 ASSUMPTIONS AND CHOICE OF MODEL.....	12
4.4 VAPOUR LIQUID EQUILIBRIUM CALCULATIONS .....	14
4.4.1 <i>Initialization</i> .....	16
4.4.2 <i>Calculation of <math>\beta</math></i> .....	16
4.4.3 <i>Calculation of fugacity</i> .....	19
4.4.4 <i>The Peng-Robinson Equation of State</i> .....	20
4.5 VERIFICATION OF THE ALGORITHM.....	22
4.6 CRUDE OIL PRODUCT PRICING .....	25
<b>5 OPTIMIZING SEPARATOR PRESSURES (WITHOUT COMPRESSORS)</b> .....	<b>27</b>
<b>6 FIELD PROCESSING OF NATURAL GAS</b> .....	<b>31</b>
6.1 COMPRESSORS .....	32
6.2 ISENTROPIC HEAD AND ISENTROPIC EFFICIENCY.....	35
6.3 PRESSURE CONTROL IN SEPARATOR S1 AND S2 .....	37
<b>7 COMPRESSOR MODELLING</b> .....	<b>39</b>
7.1 POLYNOMIAL APPROXIMATION .....	40
7.1.1 <i>Polynomial + nonlinear term approximation of the pressure ratio</i> .....	41
7.1.2 <i>Polynomial + nonlinear term approximation of the power consumption</i> .....	43
7.1.3 <i>Conclusion</i> .....	44
7.2 PHYSICAL MODELLING .....	45
7.3 DIMENSIONLESS PARAMETERS .....	47
7.3.1 <i>Algorithm for calculating the optimal exponents of S</i> .....	49
7.3.2 <i>Calculation of discharge pressure and power consumption</i> .....	50
7.4 ANTI-SURGE CONTROL .....	52
7.5 COMPRESSOR C4.....	54
<b>8 OPTIMIZING SEPARATOR PRESSURES (WITH COMPRESSORS)</b> .....	<b>57</b>
<b>9 CONCLUSIONS</b> .....	<b>63</b>

<b>10</b>	<b>APPENDIX.....</b>	<b>65</b>
10.1	LINEAR LEAST-SQUARES PROBLEM .....	65
10.2	RESERVOIR FLUID COMPOSITION .....	66
10.3	CHEMICAL PROPERTIES .....	68
10.4	INLET CONDITION FOR THE COMPRESSOR CHARACTERISTICS .....	68
10.5	SIMPLE PI CONTROL WITH ANTI-WINDUP .....	69
10.6	PSEUDOCODE FOR BRUTE FORCE OPTIMIZATION OF A GAS OIL SEPARATION PLANT .....	70
10.7	ENCLOSED FILES .....	71
10.8	ACRONYMS.....	72
<b>11</b>	<b>BIBLIOGRAPHY .....</b>	<b>73</b>

# 1 Introduction

This Msc thesis will investigate the potential benefits of using adapting pressure set-points for the separators in a multistage crude oil production plant. One of the two multistage crude oil production plants on Snorre A is used as a case study. The standard control method for a multistage crude oil production plant is to use fixed pressure set-points for the separators. Snorre A uses this method in its current control system.

The plant investigated in this thesis processes the reservoir fluid from the subsea production system Vigdis. Vigdis is connected to eight wells and the production rates from these wells are controlled independently. The production ratio between the wells varies and this influences the inlet flow and composition to the multistage crude oil production plant

By changing the separator pressure the multistage crude oil production plants adapts to this new inlet condition. A steady state model of the multistage crude oil production plant is derived and this model is used to find the optimum separator pressures. The optimum separator pressures are found by brute force optimization. MATLAB is used to implement both the steady state simulation model and the brute force optimization.

Optimizing separator pressure will increase oil production since fewer hydrocarbons, more than 2 carbon molecules, are lost to the gas phase. Snorre A produces more than 200 000 barrels per day and even a marginal percentage increase in the oil production will therefore be profitable.

This thesis has two main parts. In the first part, chapter 2-5, a multistage crude oil production plant without gas compression is studied. In this plant the reservoir fluid is separated into gas and crude oil and the optimum separator pressure is found. The optimum separator pressures are the pressures that maximise the income from the crude oil sale.

In the second part, chapter 6-9, a multistage crude oil production plant with gas compression is studied. The gas from the separators must be compressed before it can be sold or injected back to the reservoir. Compression consumes huge amount of energy and the feasible region for the separator pressures is reduced. The energy cost of operating the compression plant is added to the object function and the optimum separator pressures is found.

## ***1.1 Placement in the overall control structure***

According to Hovd (2008), control systems in the process industries can be divided into four main groups: regulatory control, supervisory control, real time optimization and production planning/scheduling. Hovd describes the real time optimization group as:

- **Real Time Optimization (RTO)**

The RTO layer identifies the optimal conditions by solving an optimization problem involving models of the production cost, value of product (possibly dependent on quality), and the process itself. The process model is often non-linear and derived from fundamental physical and chemical relationships, but they are usually static.

The control method implemented in this thesis uses an optimization problem to maximize the profit for a multistage crude oil production plant. The model is derived from non-linear fundamental physical and chemical relationships and the method is therefore clearly a part of the real time optimization group.

A dynamic model would have complicated both the derivation of the model and the solution method. This would have required non-linear model predictive control and according to Hauger (2008) only eight companies in the world uses this technology. A dynamic model is therefore too comprehensive for this thesis and a steady state model will be used.

## ***1.2 Contributions of this thesis***

The contributions of this thesis can be summarized as follows:

- **Separator modelling:** The literature review on separator modelling and implementation of the vapour liquid equilibrium routine in MATLAB. Compression between the MATLAB implantation and UNISM design.
- **Optimizing separator pressures (without compressors):** Implantation of the brute force optimization. The idea of optimising the separator pressures for a multistage crude oil production plant has been published before, see Bahadori, Vuthaluru & Mokhatab (2008).
- **Field processing of natural gas:** The adjustments of the compressor models so that they fit the actual compressor characteristics from Snorre A. This includes the polynomial plus nonlinear term approximation, algorithm for calculating the optimal exponent of S, and the parameter estimation routine implemented in MATLAB. The extension of the dimensionless parameters model to include surge control.
- **Optimizing separator pressures (with compressors):** An extension of the multistage crude oil production plant has been derived to take the gas compression into account. The brute force optimization of the separator pressures for this plant.

## 2 Gas oil separation plant

At the high pressure existing at the bottom of the producing well, crude oil contains great quantities of dissolved gases (Abdel-Aal et al, 2003). The weight of the reservoir fluid and friction in the production string reduces the inlet pressure for the gas oil separation plant. Some of the lighter hydrocarbons will change phase and bubbles will form in the fluid. The fluid is now unstable and some means of separation must be provided.

The crude oil from the reservoir is processed into gas and oil in the three separators, see Figure 1. This has to be done offshore because the crude oil from the well is unstable and not suitable for transport. The first separator operates at a high pressure and the pressure is reduced each time the oil enters a new separator. The pressure in the third separator must be near atmospheric pressure so that the oil can be stored in barrels, tankers or atmospheric reservoir.

The reservoir fluid on Snorre A contains water and separator S2 is replaced with a three phase separator for the actual process. This thesis assumes that the fluid consists of hydrocarbons and nitrogen and a two phase separator will therefore be used.

The production rate through the system is controlled by the choke valve placed before separator S1. On Snorre A this choke valve is adjusted manually. A change in pressure for separator S1 will therefore affect the production rate.

This is not desired and it is therefore assumed that this valve opening is controlled such that the production rate is constant. This thesis assumes that the production rate is measured and controlled by the flow controller: FC-S11. Unfortunately, the reservoir fluid is a multi-phase flow and is therefore difficult to measure. For more information on multi-phase flow measurements consult Ismail, Gamio, Bukharia, & Yang (2005). It is assumed that the pressure at the wellhead is high and the pressure in separator S1 can be increased to 45 bars without reducing the production rate.

Pressure in the three separators is controlled by a valve on the outlet gas flow. The valve opening is controlled by a PI controller and the current control system uses a fixed set-point of 36, 12 and 2 bar for the first, second and third stage separator, respectively. Liquid level in the three separators is controlled by a valve on the outlet crude oil flow.

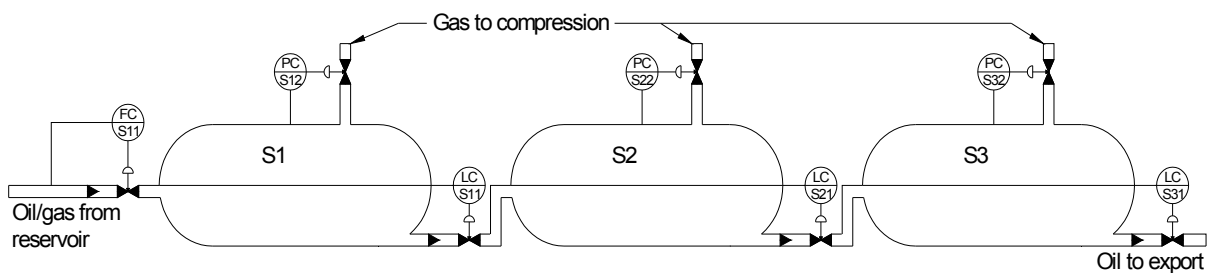


Figure 1: PI&D for a gas oil separation plant.

The well stream contains essentially three main groups of hydrocarbons and the three main groups are:

1. Light group, which consists of methane (CH<sub>4</sub>) and ethane (C<sub>2</sub>H<sub>6</sub>)
2. Intermediate group, which consists of two subgroups: the propane/butane (C<sub>3</sub>H<sub>8</sub>/C<sub>4</sub>H<sub>10</sub>) group and the pentane/hexane (C<sub>5</sub>H<sub>12</sub>/C<sub>6</sub>H<sub>14</sub>) group.
3. Heavy group, which is the bulk of crude oil and is identified as hydrocarbons with seven or more carbon atoms per molecule.

In carrying out the gas-oil separation process, the main target is to try to achieve the following objectives:

1. Separate the C<sub>1</sub> and C<sub>2</sub> light gasses from oil. Heavier hydrocarbons tend to condense, forming two-phase flow and thus creating pipeline operating problems
2. Maximize the recovery of heavy components of the intermediate group in crude oil
3. Save the heavy group components in liquid product. (Abdel-Aal et al 2003: 60)

The preferred gas-oil separation method with respect to the objectives above is differential or enhanced separation. In this method a sample of the reservoir fluid is placed in a cylinder with a gas valve at the top. The liberated gas is slowly removed from the oil through the gas valve. As pointed out by Clark (1960), when the gas is separated in this manner, the maximum amount of heavy and intermediate components will remain in the liquid, minimum shrinkage of the oil will occur, and, therefore, greater stock-tank oil recovery will occur.

According to Ahmed (2006), this is due to the fact that the gas liberated earlier at higher pressures is not present at lower pressures to attract the intermediate and heavy components and pull them into the gas phase. Nevertheless, commercial separation based on differential concept is very costly and is not a practical approach (Abdel-Aal et al 2003).

The gas-oil separation method used on Snorre A and in this thesis is flash or equilibrium separation. This method reduces the pressure in steps, see Figure 1. When more stages are added the oil recovery increases and the power needed to compress the gas for export or injection is reduced, see Table 1. Adding an extra stage is a large investment since this requires additional separator, compressor, piping and control systems. In most cases, the optimum number of stages is very difficult to determine as it may be different from well to well and it may change as the wells' flowing pressure declines with time, (Arnold & Stewart 1999).

**Table 1: Effect of separation pressure for a rich condensate stream (from (Arnold & Stewart 1999))**

Case	Separation stages [bar]	Liquid Produced [bps]	Compressor horsepower required
I	84,4.4	8.400	861
II	84,36,4.4	8.496	497
III	84,36,14.4.4	8.530	399

## 2.1 Optimum pressure for gas-oil separators

The pressure in the separators will influence the oil recovery and this is demonstrated with an example. In this example the reservoir fluid is flashed in an initial separator and then the liquid from this separator is flashed again at the stock tank. The pressure in the stock tank is 1 bar.

The oil recovery is calculated by using the method presented in Section 4.4. Figure 2 presents the effect of initial separator pressure on the oil recovery. Where, Fluid 1 has a high gas oil ratio, Fluid 2 has an average gas oil ratio and Fluid 3 has a low gas oil ratio. The exact composition of these fluids is presented in Section 10.2.

Figure 2 shows that the oil recovery is dependent on the initial separator pressure and the reservoir fluid composition. An initial separator pressure of 17 [bar] gives the maximum oil recovery for a reservoir fluid with high gas oil ratio. The initial separator pressure must be reduced to obtain maximum oil recovery for a reservoir fluid with lower gas oil ratio.

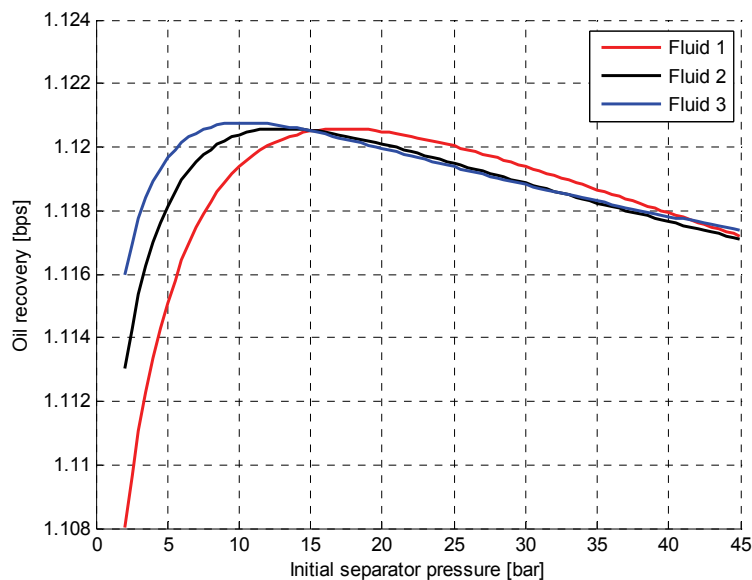


Figure 2: Effect of initial separator pressure on the oil recovery.

This thesis will use vapour liquid equilibrium calculation to determine the optimum pressure for the gas-oil separators. In Section 2.1.1 an empirical method is used to determine the optimal second-stage operation pressure is presented. The main drawback with this method is that it assumes that the first-stage separator pressure is constant.

### 2.1.1 Empirical method

In a gas oil separation plant with three separators the optimum second stage pressure can be calculated with a method proposed by Whinery, K. F. & Compbell, J. M. (1958). The optimal second stage pressure is the pressure that maximizes the oil yield. In this method the first stage pressure is assumed known and the third stage pressure is near atmospheric pressure.

$$P_{2,o} = \begin{cases} 16.04 \cdot AP_1^{0.686} + 29.58 \cdot 10^4 (A - 0.057) & \text{if } M > 1 \\ 7.981 \cdot AP_1^{0.765} + 57.43 \cdot 10^4 (A + 0.028) & \text{if } M \leq 1 \end{cases} \quad (2.1)$$

$$M = \frac{MW_{ws}}{MW_{air}} \quad (2.2)$$

Where  $P_{2,o}$  is the optimum pressure [bar] in the second stage separator,  $P_1$  is the pressure [bar] in the first stage separator,  $MW_{ws}$  is the molecular weight of the well stream and  $MW_{air}$  is the molecular weight of air.  $A$  is a dimensionless constant evaluated from Figure 3 using  $M$  and the parameter  $Z$ . The parameter  $Z$  is the sum of mole fractions of the hydrocarbons  $C1+C2+C3$  found in the well stream. The black lines in Figure 3 are for different values of  $Z$ .

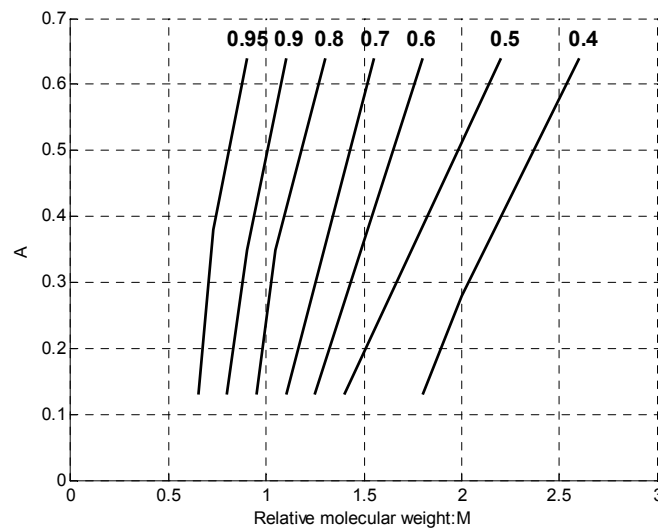


Figure 3: Determination of the A factor.





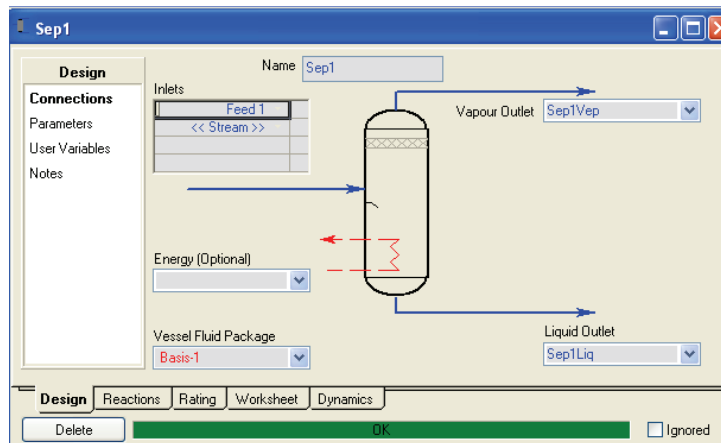


Figure 5: Configuration window for two-phase separator in UNISIM Design.

An implementation in UNISIM Design will have small second hand value for Siemens since they have to buy a license for this software and purchase is very expensive. A MATLAB implementation can be used by Siemens and can be compiled to C. This makes it easier to implement the system in a future control system. UNISIM Design can also be linked to the control system by using an OPC server. In this case a computer with UNISIM Design must be connected to the control system.

In UNISIM Design the designer is bound to the methods that exist in the program. MATLAB can implement any method and this gives greater flexibility. For example flash calculations appearing in commercial process simulators are based on local minimization, (Saber & Shaw, 2007). If MATLAB is chosen a global minimization method can be implemented.

This project will be implemented in MATLAB since this gives a larger second hand value for Siemens and offers more flexibility. UNISIM design will be used to verify the phase equilibrium method implemented in MATLAB.

## 4 Separator modelling

The separator will be modelled by using phase equilibrium calculations. In phase equilibrium calculation, a thermodynamic model and an optimization algorithm must be chosen. A thermodynamic model gives the relation between pressure, molar volume and temperature for pure components and mixtures. The thermodynamic model is usually nonlinear and nonconvex and therefore an optimization method must be used to find phase equilibrium. These two routines can in most cases be selected independently of each other.

From Carroll (2003) the criteria for phase equilibrium are defined as: (1) the temperature and pressure of the phases are equal, (2) the chemical potentials of each of the components in each of the phases are equal and (3) the global Gibbs free energy is a minimum. Phase equilibrium was first established by Gibbs for more than 100 years ago.

Most phase equilibrium calculations switch from chemical potentials to fugacities, (Carroll, 2003). The fugacity is a property created by G.N Lewis to provide an alternative to the chemical potential. Conceptually, fugacity offers no advantage over the chemical potential, but it does offer computational advantages, particularly for mixtures, (O'Connell & Haile, 2005).

### 4.1 Optimization algorithm

Current frameworks to solve the phase equilibrium problem can be divided into two main types: indirect and direct minimization, Vázquez-Román et al (2000). The indirect minimization only uses criteria 1 and 2 for phase equilibrium and hopes this will also satisfy criteria 3.

Direct minimization method finds the global or local minimum of the Gibbs free energy when criteria 1 is satisfied. Because the Gibbs free energy of the system is a minimum at equilibrium, several researchers have adopted optimization techniques to minimize this property directly for a specified number of phases (Chaikunchuensakun, Stiel, & Baker, 2002). Direct minimization can further be divided into two groups: local and global. Global direct minimization fulfils all three criteria for phase equilibrium. The local direct minimization fulfils criteria one, two and a local minimum of the Gibbs free energy.

#### 4.1.1 Indirect minimization

According to Vázquez-Román et al (2000) the successive substitution (SS) method is the most popular method that has proved to converge to the optimal in most practical cases. However, a good initial estimation is required to avoid undesired solutions and enhance convergence. Since the SS method always converges to a local minimum of the Gibbs free energy, all three criteria for phase equilibrium are satisfied (Michelsen, 1982).

One weakness with the SS method is that it has linear rate of convergence and that for near-critical region, the rate of convergence becomes extremely slow (Firoozabadi, 1999). Many methods have been proposed to accelerate the convergence rate of SS method. In petroleum reservoir simulations, phase equilibrium calculation routine represents a key sequence and a huge number of flash calculations are performed (Nichita, Gomez, & Luna, 2002).

In the works of Vázquez-Romanán et al (2000) and Mehra et al (1982) an accelerated successive substitution method was used and the rate of convergence was improved substantially. However, a common weakness of all acceleration methods is that Gibbs free energy may increase during the iteration and eventually converge to a false or trivial solution. When an increase in the Gibbs free energy is detected the algorithm switches to a Newton method. The Newton method has quadratic convergence, but needs a better initial estimate of the equilibrium values (Firoozabadi, 1999). To guarantee a descent direction the hessian must be positive definite. In the algorithm proposed by Vázquez-Romanán et al (2000) the hessian is maintained symmetric and positive definite by the Levenberg-Marquardt method.

#### **4.1.2 Local direct minimization**

Chaikunchuensakun, Stiel, & Baker (2002) proposed a combined algorithm for stability and phase equilibrium by Gibbs free energy minimization.

Nichita, Broseta, & Hemptinne (2006) proposed a method for multiphase equilibrium calculations that uses reduced variables. This is possible since the number of independent variables for phase equilibrium calculations does not depend on the number of components in the mixture. For this method the computer time increases somewhat linearly with the number of components, while for standard methods this dependence is at least quadratic.

#### **4.1.3 Global direct minimization**

Since the equation of states in general is a non-convex nonlinear function, many local optimums can exist. The algorithms that fall into this category try to find the global minimum of the Gibbs free energy. According to (Harding & Floudas, 1999) the difficulty of locating the global minimum of the Gibbs free energy is due to two main points: 1) there is no method to determine a priori the number and types of phases present in the equilibrium state, and 2) for nonideal systems the Gibbs energy surface may contain multiple local minima.

Rossi, Cardozo-Filho, & Guirardello (2009) proposed an approach for the minimization of the Gibbs free energy using linear programming that guarantees finding the global optimum within some level of precision, for any kind of thermodynamic model. For systems with more than four components the calculation time and memory requirements becomes too excessive and the completion of the calculations is not feasible.

In the work of Zhu, Wen, & Xu (2000) an enhanced simulated annealing algorithm is presented to verify the phase stability analysis and obtain the true solution of the phase equilibrium problem of multi-component systems at high pressures.

According to Nichita et al (2002) a global optimization method called Tunneling, able to escape from local minima and saddle points, is used here, and has shown to be able to efficiently find the global solution for all the hypothetical and real problems tested. The Tunneling method has two steps. In step one, a local bounded optimization method is used to minimize the objective function. In step two (tunnelization), either global optimality is ascertained, or a feasible initial estimate for a new minimization is generated.

Harding & Floudas (1999) used the deterministic global optimization algorithm  $\alpha$ -based Branch and Bound to find chemical equilibrium. The key idea is the construction of a converging sequence of upper and lower bound on the global minimum through the convex relaxation of the original problem, Adjiman et al (1997). In this work a system of eight hydrocarbons was studied and the algorithm used 7.5 minutes to converge to the global minimum.

## ***4.2 Thermodynamic models***

There exist three main types of thermodynamic models: The virial equations, equations of states and activity coefficient models. For more information on thermodynamic models, consult (Assael, Trusler, & Tsolakis, 1996).

According to Honeywell (2008), equation of state models have proven to be very reliable in predicting properties of most hydrocarbon-based fluids over a large range of operating conditions, and their application has been limited to primarily non-polar or slightly polar components. The equation of state models is also the only model that can be used to estimate thermodynamic properties for both the liquid and vapour phases.

For mixtures containing polar components, for example water, the activity coefficient method is more accurate (Assael, Trusler, & Tsolakis, 1996). According to Honeywell (2008), activity models are much more empirical in nature when compared to the property predictions in the hydrocarbon industry. For this reason, they cannot be used as reliably as the equations of state for generalized application or extrapolated into untested operating conditions. Their adjustable parameters should be fitted against a representative sample of experimental data and their application should be limited to moderate pressures.

According to (Adewumi), the Peng Robinson Equation of State (EOS) has become the most popular EOS for natural gas systems in the petroleum industry. This EOS is also used by Bahadori, Vuthaluru, & Mokhatab (2008) who proposed a method for optimizing separator pressures in the multistage crude oil production unit.

### **4.3 Assumptions and choice of model**

The first assumption is that the reservoir fluid contains no polar components. A typical reservoir fluid contains the polar components: water, hydrogen sulfide and carbon dioxide. Hydrogen sulfide and carbon dioxide can quite easily be included by using a group contribution method, see Privat, Jaubert, & Mutelet (2008). To be able to include water, a method that handles vapour liquid liquid equilibrium must be used and the activity coefficient model must be used for the liquid phases. It is therefore possible to use the Peng Robinson EOS for both the vapour and liquid phases, and this is the approach that will be used in this project.

Figure 6 presents the phase envelope for the three separators at Snorre A. The phase envelope is valid for the operation condition specified in Section 4.5 at page 22. According to Adewumi the dew point, bubble point and critical point can be defined as: Dew point is the pressure and temperature condition at which an infinitesimal quantity of liquid (a droplet) exists in equilibrium with vapour. Bubble point is the pressure and temperature condition at which the system is all liquid, and in equilibrium with an infinitesimal quantity (a bubble) of gas. Critical point is the temperature and pressure for which liquid and vapour are indistinguishable.

Operation condition is the pressure and temperature for separators S1, S2 and S3. L is the liquid region. In the two-phase region (L+V) both a liquid and vapour phase exists and V is the vapour region.

From the reservoir to the first separator and between the separators a considerable pressure reduction occurs. It is therefore reasonable to assume that the fluid separates into a liquid and vapour phase. This is also confirmed in Figure 6 where the operation condition for separator S1, S2 and S3 is placed well inside the two phase region. This simplifies the problem from phase equilibrium calculation to vapour liquid equilibrium calculation.

In this application the number of vapour liquid equilibrium calculation needed is quite small and the sampling time is large, approximately one hour. Figure 6 shows that the operation condition is far from the critical point and the SS method can therefore be used. Since speed is not important, the successive substitution method is used. The SS method is the most popular, best documented and easiest to implement. The third and final assumption is that the local solution found by the SS method is the global solution.

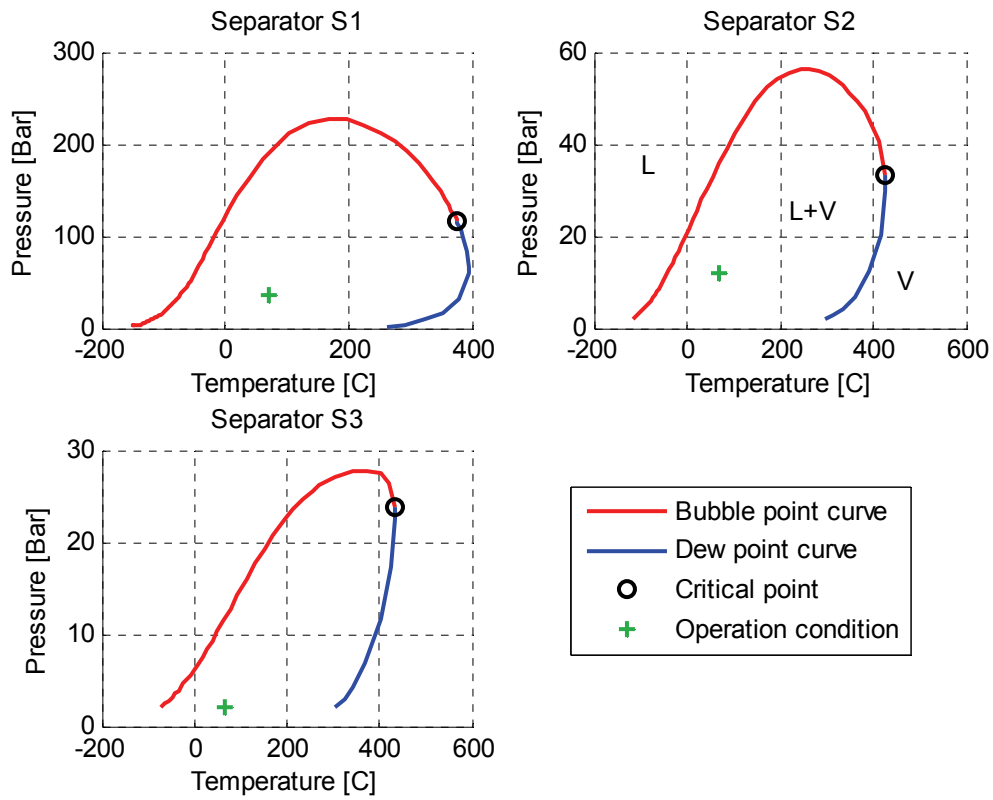


Figure 6: Phase envelope for separator S1, S2 and S3 (calculated in UNISIM Design).

#### 4.4 Vapour liquid equilibrium calculations

A flash process is one in which a fluid stream of known compositions and flow rate passes through a throttle and into a vessel where liquid and vapour phases are separated before passing through the appropriate outlet (Assael, Trusler, & Tsolakis, 1996).

In this project an iterative algorithm is used to find the vapour liquid equilibrium. The algorithm is mostly based on the course phase relations in reservoir engineering taught at the Pennsylvania State University, see Adewumi. Some tips on how to implement the algorithm in MATLAB are taken from Rosales-Quintero who has implemented an isothermal flash calculation algorithm in MATLAB using Soave equation of state. The books Assael, Trusler, & Tsolakis (1996) and Wauquier (2000) also recommends the method proposed by Adewumi for solving isothermal flash calculations.

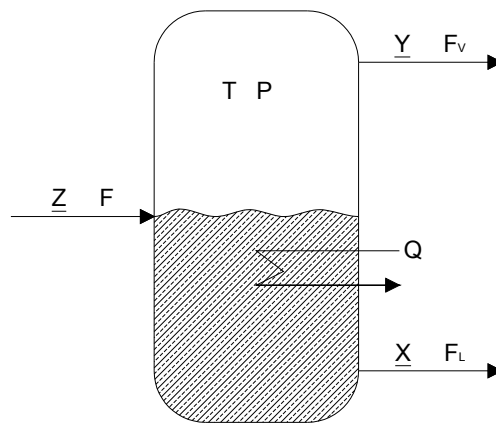


Figure 7: Isothermal flash unit.

In Figure 7 a typical overview of an isothermal flash unit is shown. Where  $\underline{Z}$  is the molar composition of the inlet flow,  $\underline{Y}$  is the molar composition of the vapour outlet flow,  $\underline{X}$  is the molar composition of the liquid outlet flow,  $T$  is the temperature,  $P$  is the pressure,  $Q$  is the heat flow,  $F$  is the inlet molar flow,  $F_v$  is the outlet vapour molar flow and  $F_L$  is the outlet liquid molar flow. The underlining under the letters  $Y$ ,  $Z$  and  $X$  is used to specify that these values are vectors with one number for each component of the inlet stream.

According to (Assael, Trusler, & Tsolakis, 1996), the operating pressure of the unit is controlled in some way and heat is supplied or removed at rate  $Q$  through a heat exchanger so as to maintain isothermal conditions at temperature  $T$ . The known parameters are  $T$ ,  $P$ ,  $\underline{Z}$  and  $F$  and the unknown parameters are  $\underline{Y}$ ,  $\underline{X}$ ,  $F_v$  and  $F_L$ . Since there is a relation between the unknown parameters, the problem can be reduced to finding  $\underline{K}$  and  $\beta$ . This gives a problem with  $n+1$  unknown variables, where  $n$  is the number of components in the inlet stream.

In Figure 8 a block diagram of the isothermal flash calculation algorithm is presented. The algorithm consists of three main parts: initialization, calculation of  $\beta$  and calculation of fugacity.



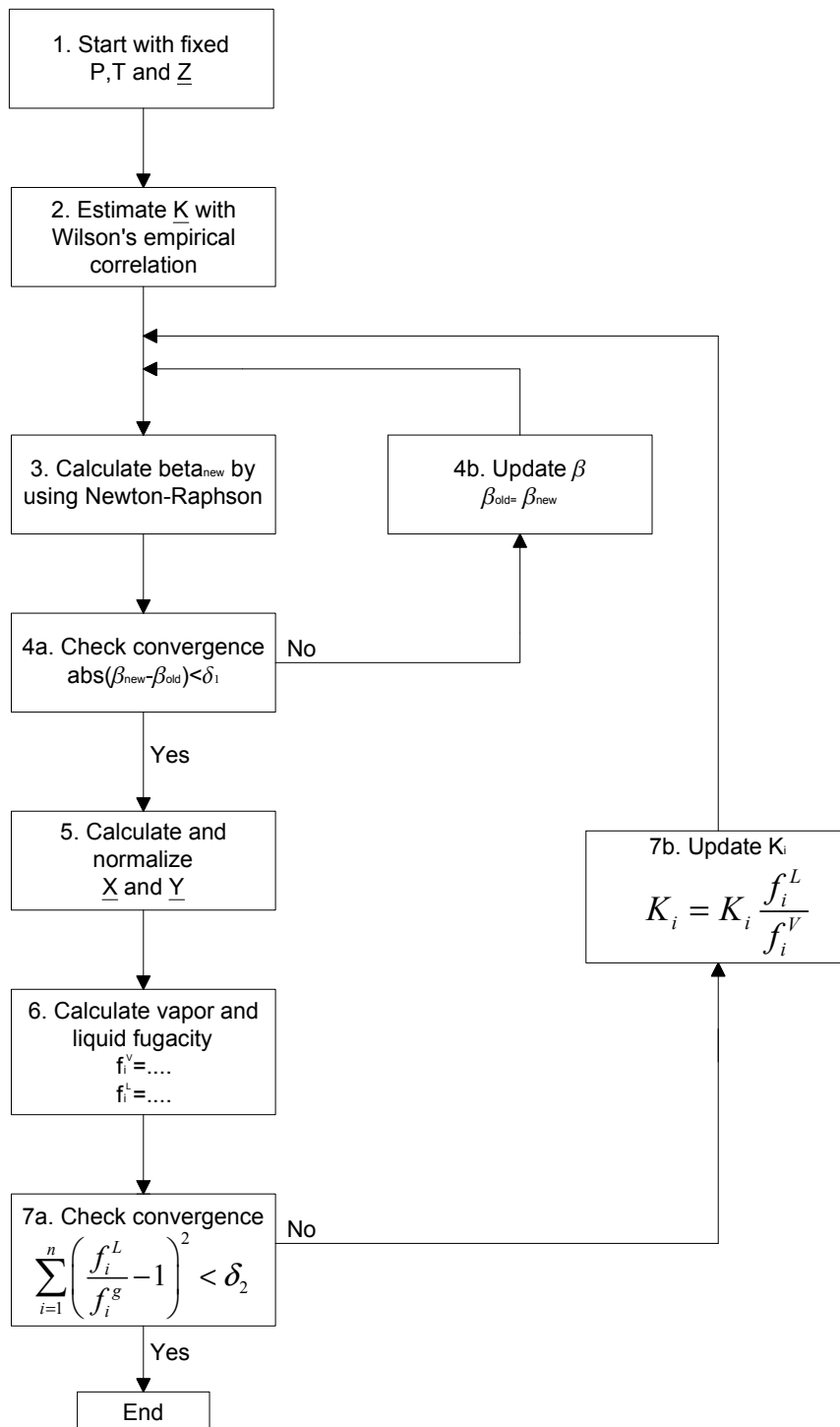


Figure 8: Flow chart of isothermal flash calculation.

#### 4.4.1 Initialization

An initial value for equilibrium ratios  $K_i$  is needed for the calculation of  $\beta$ . The Wilson's empirical correlation is a popular empirical correlation that is very often used in the petroleum and natural gas industry. This correlation gives the value of  $K_i$  as a function of reduced conditions and acentric factor, and is written as (Adewumi):

$$K_i = \frac{1}{P_{ri}} e^{5.37(1 + \omega_i)(1 - \frac{1}{T_{ri}})} \quad (4.1)$$

In Equation (4.1)  $\omega$  is the acentric factor. According to Arnold & Stewart (1999), the substance reduced properties can be calculated from the critical properties, see Equation (4.2) and (4.3). Where subscript, c is the critical value, r is reduced value and i is used to select a specific component. The critical properties and acentric factor for a fluid is constant and these values are presented in Section 10.3. Where i=1 equals nitrogen, i=2 equals methane and so forth.

$$P_{ri} = \frac{P_i}{P_{ci}} \quad (4.2)$$

$$T_{ri} = \frac{T_i}{T_{ci}} \quad (4.3)$$

#### 4.4.2 Calculation of $\beta$

This part of the algorithm calculates the vapour and liquid molar flow and composition for a constant value of the equilibrium ratios. The equilibrium ratios found by the Wilson's empirical correlation is most likely not the true equilibrium ratios and these values will be updated by the last part of the algorithm.

$$F_v = \beta F \quad (4.4)$$

$$F_L = (1 - \beta)F \quad (4.5)$$

Equation (4.4) and (4.5) describes the vapor and liquid mole flows as a function of  $\beta$  and inlet mole flow. Since only the overall composition of the mixture is known, a material balance for each of the n components is required:

$$Fz_i = F_L x_i + F_v y_i \quad (4.6)$$

$$K_i = \frac{y_i}{x_i} \quad (4.7)$$

$K_i$ , in Equation (4.7), is the equilibrium ratios. Equation (4.6) is solved with respect on  $x_i$  and the flow rates are eliminated in terms of the vapor fraction in Equation (4.4):

$$x_i = \frac{z_i}{1 + \beta(K_i - 1)} \quad (4.8)$$

$$\sum_{i=1}^n x_i = 1 \quad (4.9)$$

The summation of all molar vapor fractions must be equal to one, see Equation (4.9). In Equation (4.10) and (4.11) two possible object functions for finding  $\beta$  are presented. These two functions are non-linear and can be solved with a Newton-Raphson method. One problem with this approach is that the object functions are not monotonic and therefore the Newton-Raphson method might end up with the wrong solution.

$$f_x(\beta) = \sum_{i=1}^n \left( \frac{z_i}{1 + \beta(K_i - 1)} \right) - 1 = 0 \quad (4.10)$$

$$f_y(\beta) = \sum_{i=1}^n \left( \frac{z_i K_i}{1 + \beta(K_i - 1)} \right) - 1 = 0 \quad (4.11)$$

Rachford & Rice (1952) solved this problem by combining the two object functions. Equation (4.13) presents the Richford Rice objective function and Equation (4.14) presents the derivative of this function. They used a binary search algorithm to find  $f(\beta)=0$ .

$$f(\beta) = f_y(\beta) - f_x(\beta) \quad (4.12)$$

$$f(\beta) = \sum_{i=1}^n \frac{z_i(K_i - 1)}{1 + \beta(K_i - 1)} = 0 \quad (4.13)$$

$$\dot{f}(\beta) = - \sum_{i=1}^n \frac{z_i(K_i - 1)^2}{(1 + \beta(K_i - 1))^2} = 0 \quad (4.14)$$

Since the composition  $z_i$  and something square is always positive the derivate of Rachford Rice objective function is always negative. It is therefore proven that the Richford Rice object function is a monotonically decreasing function. A remaining weakness of the Rachford-Rice objective function is that, although monotonic, it is not continuous at all points of the domain Adewumi. By inspection of the Rachford Rice objective function n singularities exists and they accrue if  $\beta = \beta_{\text{sing}}$ .

$$\beta_{\text{sing}} = \frac{1}{1 - K_i} \quad (4.15)$$

Equation (4.7) shows that the only physical meaningful values for  $k_i$  are values larger than zero. This is because  $k_i$  smaller than zero gives a negative mole fraction of substance  $i$  in either the vapour or liquid phase. By inspecting Equation (4.4) and (4.5) the physical meaningful values for  $\beta$  are between zero and one. Equation (4.16) proves that all the singularities are placed outside the physical meaningful region.

$$\begin{aligned}
& \text{if } (0 < K_i \leq 1) \\
& \quad B_{\text{sing}} > 1 \\
& \text{if } (1 < K_i < \infty) \\
& \quad B_{\text{sing}} \leq 0
\end{aligned} \tag{4.16}$$

In the physical meaningful region the Rachford Rice objective function is continuous and monotonically decreasing and therefore only one or zero roots to Equation (4.13) exists. In this project the Newton Raphson procedure is used to find the root of Equation (4.13). The Newton Raphson procedure is presented in Equation (4.17) from Croft, Davison, & Hargreaves (2001). Equation (4.19) ensures that  $\beta_{\text{new}}$  is in the physical meaningful region.

$$x_{i+1} = x_i - \frac{f(x_i)}{f'(x_i)} \tag{4.17}$$

$$\beta_{NR} = \beta_{old} + \frac{\sum_{i=1}^n \frac{z_i(K_i - 1)}{1 + \beta_{old}(K_i - 1)}}{\sum_{i=1}^n \frac{z_i(K_i - 1)^2}{(1 + \beta_{old}(K_i - 1))^2}} \tag{4.18}$$

$$\beta_{new} = \begin{cases} \beta_{NR} & \text{if } (0.001 < \beta_{NR} < 0.999) \\ 0.999 & \text{if } (\beta_{NR} \geq 0.999) \\ 0.001 & \text{if } (\beta_{NR} \leq 0.001) \end{cases} \tag{4.19}$$

Convergence is achieved when Equation (4.20) is satisfied.  $\delta_1$  is a small number and in this project  $\delta_1$  is equal to  $10^{-14}$ .

$$|\beta_{new} - \beta_{old}| < \delta_1 \tag{4.20}$$

If convergence is not achieved,  $\beta_{old} = \beta_{new}$  and the calculations of Equations (4.18) and (4.19) are repeated. When convergence is achieved,  $\beta_{new}$  is used to calculate the vapour and liquid composition, see Equation (4.21) and (4.22).

$$x_i = \frac{z_i}{1 + \beta_{new}(K_i - 1)} \tag{4.21}$$

$$y_i = \frac{z_i K_i}{1 + \beta_{new}(K_i - 1)} \tag{4.22}$$

The liquid and vapour compositions are normalised so that Equation (4.23) is true.

$$\sum_{i=1}^n x_i = \sum_{i=1}^n y_i = 1 \tag{4.23}$$

### 4.4.3 Calculation of fugacity

In this project the successive substitution method is used. According to Vázquez-Román et al (2000) successive substitution is the most popular method that has proved to converge to the optimal in most practical cases. However, a good initial estimation is required to avoid undesired solutions and enhance convergence.

The Peng Robinson EOS is used to calculate the partial fugacity coefficient for the vapour and liquid phase, see Section 4.4.4. In Equation (4.24) and (4.25) the fugacity of the vapour and liquid phase is calculated. For the system to be at equilibrium fugacity of component  $i$  must be equal in the vapour and liquid phase for all  $n$  components.

$$f_i^V = \varphi_i^V y_i P \quad (4.24)$$

$$f_i^L = \varphi_i^L x_i P \quad (4.25)$$

Convergence is achieved when Equation (4.26) is satisfied.  $\delta_2$  is a small number and in this project  $\delta_2$  is equal to  $10^{-14}$ . If convergence is achieved the system is at equilibrium and the isothermal flash algorithm is finished.

$$\sum_{i=1}^n \left( \frac{f_i^L}{f_i^g} - 1 \right)^2 < \delta_2 \quad (4.26)$$

In the opposite case the  $K$  values must be updated and this is done by a successive substitution method. According to Jaluria (2008) a particularly simple method for root solving is the successive substitution method, in which the given equation  $f(x) = 0$  is rewritten as  $x = g(x)$ . At the root,  $\alpha = g(\alpha)$ , where  $\alpha$  is the root of the original equation and thus  $f(\alpha) = 0$ . This yields an iterative scheme given by the equation:

$$x^{k+1} = g(x^k) \quad (4.27)$$

At equilibrium the fugacity of the vapour and liquid phase is equal for all  $n$  components ( $f_i^L = f_i^V$ ) and therefore:

$$K_i = \frac{\varphi_i^L}{\varphi_i^V} \quad (4.28)$$

By using the successive substitution method on Equation (4.28) an iterating scheme for updating  $K_i$  can be found.

$$f(K_i) = \frac{\varphi_i^L}{\varphi_i^V} - K_i = 0 \quad (4.29)$$

This gives:

$$K_i = g(K_i) = \frac{\varphi_i^L}{\varphi_i^V} \quad (4.30)$$

By inserting Equation (4.30) into Equation (4.27) and substituting x with K and iterative scheme for updating  $K_i$  is found:

$$K_i^{k+1} = \frac{\phi_i^L}{\phi_i^V} = \frac{x_i P}{\frac{f_i^V}{y_i P}} = \frac{f_i^L y_i}{f_i^V x_i} = K_i^k \frac{f_i^L}{f_i^V} \quad (4.31)$$

The old  $K_i$  values are not needed and the updating rule can therefore be simplified to Equation (4.32). If convergence is not achieved the  $K_i$  values are updated as seen in Equation (4.32) and the algorithm returns to step 3 in Figure 8.

$$K_i = K_i \frac{f_i^L}{f_i^V} \quad (4.32)$$

#### 4.4.4 The Peng-Robinson Equation of State

The Peng & Robinson (1976) Equation of State with one modification is used to calculate the fugacity coefficient. The PR is a modification of the Redlich Kwong (RK) Equation of State which corresponds to a lower critical compressibility of about 0.307 thus representing the VLE of natural gas systems accurately, (Honeywell 2008).

In Equation (4.33) to (4.44) the Peng Robinson equation of state is presented. Where, P is the pressure,  $\phi_i$  is the fugacity coefficient, R is the universal gas constant, T is the temperature,  $V_m$  is the molar volume,  $m_i$  is the molar fraction of component i in either the vapor or liquid phase,  $k_{ij}$  is the binary interaction parameter and Z is the compression factor.

$$P = \frac{RT}{V_m - b} - \frac{a\alpha}{V_m(V_m + b) + b(V_m - b)} \quad (4.33)$$

$$Z^3 - (1 - B)Z^2 + (A - 3B^2 - 2B)Z - (AB - B^2 - B^3) = 0 \quad (4.34)$$

$$A = \sum_{i=1}^n \sum_{j=1}^n m_i m_j (1 - k_{ij}) \sqrt{A_i A_j} \quad (4.35)$$

$$B = \sum_{i=1}^n m_i B_i \quad (4.36)$$

$$a\alpha = \sum_{i=1}^n \sum_{j=1}^n m_i m_j (1 - k_{ij}) \sqrt{a_i \alpha_i a_j \alpha_j} \quad (4.37)$$

$$b = \sum_{i=1}^n m_i b_i \quad (4.38)$$

$$A_i = 0.45724 \alpha_i \frac{P_{r,i}}{T_{r,i}^2} \quad B_i = 0.07780 \frac{P_{r,i}}{T_{r,i}} \quad (4.39)$$

$$a_i = 0.45724 \frac{(RT_i^c)^2}{P_i^c} \quad b_i = 0.07780 \frac{RT_i^c}{P_i^c} \quad (4.40)$$

$$\alpha_i = \left[ 1 + n_i \left( 1 - \sqrt{T_{r,i}} \right) \right]^2 \quad (4.41)$$

In the original PR EOS Equation (4.42) was used for all  $\omega_i$ . According to Danesh (1998) this correlation was later modified to improve predictions for heavier components, see Equation (4.42) and (4.43).

$$\text{if } (\omega_i \leq 0.491) \quad n_i = 0.37464 + 1.54226\omega_i - 0.26992\omega_i^2 \quad (4.42)$$

$$\text{if } (\omega_i > 0.491) \quad n_i = 0.379642 + 1.48503\omega_i - 0.164423\omega_i^2 + 0.016666\omega_i^3 \quad (4.43)$$

$$\begin{aligned} \ln \phi_i &= \frac{B_i}{B} (Z - 1) - \ln(Z - B) \\ &+ \frac{A}{2.828B} \left[ \frac{B_i}{B} - \frac{2}{a\alpha} \sum_{j=1}^n m_j (1 - k_{ij}) \sqrt{a_i \alpha_i a_j \alpha_j} \right] \ln \left( \frac{Z + 2.414B}{Z - 0.414B} \right) \end{aligned} \quad (4.44)$$

When the fugacity coefficient of the liquid phase is calculated the smallest real root of Equation (4.34) is used and  $m_i = x_i$ . For the fugacity coefficient of vapor phase the largest real root of Equation (4.34) is used and  $m_i = y_i$ .

Equation (4.37) and (4.38) is the classical mixing rule derived from the van der Waals theory, Wauquier (2000). Several different mixing rules exist and in the review article by Ghosh (1999) seventeen different mixing rules were discussed.

The binary interaction parameter  $k_{ij}$  is symmetric ( $k_{ij} = k_{ji}$ ) for the classical mixing rule, but for some mixing rules they are taken to be asymmetric (Ghosh 1999). In this thesis it is assumed that the binary interaction parameters are zero.

The binary interaction parameter can be estimated with a group contribution method proposed by Privat, Jaubert, & Mutelet (2008). This method makes it possible to estimate  $k_{ij}$  for any mixture containing saturated hydrocarbons (n-alkanes and branched alkanes), aromatic hydrocarbons, cyclic hydrocarbons (naphthenes), carbon dioxide, nitrogen, and hydrogen sulfide whatever the temperature.

## 4.5 Verification of the algorithm

A process with three separators in series, see Figure 9, is used to verify the vapour liquid equilibrium algorithm implemented in MATLAB. Figure 9 presents the implementation of this process in UNISIM Design. Fluid 2, see Table 12, is used as the reservoir fluid and the flow rate is 2791 [kmol/h]. Operation conditions for the three separators are presented in Table 2.

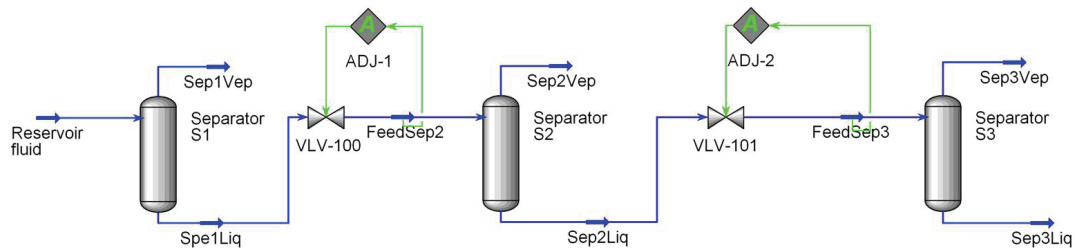


Figure 9: Separator train process.

Table 2: Operation conditions.

Separator	Pressure [Bar]	Temperature [C]
S1	36	70
S2	12	68.71
S3	2	66.11

In UNISIM Design a number of different thermodynamic models can be selected. According to (Honeywell, 2008) the PR equation of state is the ideal for VLE calculations as well as calculating liquid densities for hydrocarbon systems. UNISIM Design has an improved PR equation of state that extends its range of applicability and to improve its predictions for some non-ideal systems.

Table 3 presents the result from vapour liquid equilibrium calculations in MATLAB and UNISIM Design. Where:

- PRM1: Vapour liquid equilibrium algorithm implemented in MATLAB with critical properties and acentric factor from Yaws (1999) and all binary interaction parameters set to zero.
- PRM2: Vapour liquid equilibrium algorithm implemented in MATLAB with critical properties and acentric factor from UNISIM Design and all binary interaction parameters set to zero.
- PRU: Simulation in UNISIM Design with PR equation of state with all binary interaction parameters set to zero
- IPRU: Simulation in UNISIM Design with improved PR equation of state with binary interaction parameters estimated by UNISIM Design



Table 3 shows that the three methods PRM1, PRM2 and PRU generate comparable results. Equation (4.45) presents the method for calculating the average relative error between method m and n.

The average relative error between the PRM1 and PRU method is 0.59%. When the results from PRM2 and PRU method is compared the average relative error is 0.13%. This error is most likely caused by differences in implementation. The implementation in UNISIM design is secret and further investigation of this error is not possible.

This project will continue to use the critical properties and accentric factor presented by Yaws (1999). This is because UNISIM Design values may be copyright and this project could not find the source for these values.

The average relative error between the PRM1 and IPRU method is 14.8%. This shows that the binary interaction parameters are important and that these values should not be set equal to zero. How to estimate the binary interaction parameters is outside the scope of this project.

$$\begin{aligned}
 \Delta K_i &= \left| \frac{K_{i,m} - K_{i,n}}{\frac{(K_{i,m} + K_{i,n})}{2}} \right| 100 \\
 \Delta F_L &= \left| \frac{F_{L,m} - F_{L,n}}{\frac{(F_{L,m} + F_{L,n})}{2}} \right| 100 \\
 E &= \frac{1}{N+1} \left( \sum_{i=1}^N \Delta K_i + \Delta F_L \right)
 \end{aligned} \tag{4.45}$$

**Table 3: Comparison of VLE calculation in MATLAB and UNISIM Design.**

Separator	Method	K <sub>1</sub>	K <sub>2</sub>	K <sub>3</sub>	K <sub>4</sub>	K <sub>5</sub>	K <sub>6</sub>	K <sub>7</sub>	K <sub>8</sub>	K <sub>9</sub>	K <sub>10</sub>	F <sub>L</sub>
<b>S1</b>	PRM1	13.31	6.29	1.89	0.7774	0.4118	0.3221	0.1675	0.1395	0.0608	3.12E-05	1.23E+03
	PRM2	13.43	6.368	1.893	0.7778	0.4098	0.3212	0.167	0.1382	0.061	3.03E-05	1.23E+03
	PRU	13.42	6.333	1.893	0.7778	0.4095	0.321	0.1672	0.1384	0.061	3.04E-05	1.23E+03
	IPRU	15.66	7.419	2.282	0.9287	0.4724	0.3752	0.1903	0.1576	0.0675	2.75E-05	1.17E+03
<b>S2</b>	PRM1	39.38	17.63	4.763	1.799	0.8897	0.6841	0.3318	0.2719	0.1087	2.32E-05	1.05E+03
	PRM2	39.73	17.85	4.779	1.802	0.886	0.683	0.3305	0.2698	0.1094	2.28E-05	1.05E+03
	PRU	39.69	17.74	4.778	1.802	0.8851	0.6822	0.3309	0.2699	0.1093	2.28E-05	1.05E+03
	IPRU	46.61	20.95	5.845	2.194	1.045	0.8176	0.3878	0.317	0.1255	2.32E-05	1.02E+03
<b>S3</b>	PRM1	235.9	102.1	25.86	9.27	4.398	3.344	1.555	1.262	0.4782	6.02E-05	925.7
	PRM2	238	103.4	25.95	9.288	4.38	3.339	1.548	1.252	0.482	5.91E-05	925.8
	PRU	237.8	102.8	25.94	9.284	4.374	3.335	1.55	1.252	0.4814	5.91E-05	925.8
	IPRU	281.3	122.6	32.26	11.54	5.283	4.093	1.866	1.512	0.5703	6.48E-05	914.1

The calculation time for this example is 30 millisecond on a HP Pavilion DV6185 computer with a 1.83 GHz processor. Table 4 presents the number of iterations need for the PRM1 method to converge. The relative high numbers of iterations in the inner loop implies that the method can be improved to reduce computation time. This is not necessary since the method is fast enough for this project.

**Table 4: Iteration numbers for VLE algorithm implemented in MATLAB.**

Separator:	Iterations of outer loop	Average iterations of inner loop
<b>S1</b>	7	15
<b>S2</b>	6	17
<b>S3</b>	4	17

## 4.6 Crude oil product pricing

Crude oil produced in the gas oil separation plant is sold on the international market. The price of this product is influenced by many independent factors, where the most important factor is the relation between supply and demand. Crude oils differ in quality and this influences the price. Crude oil is categorized primarily according to their API gravity and then the sulphur content. The amount of entrained water is an additional factor for discounting the price. (Mian 2002)

API gravity measures the relative density of the petroleum fluid and can be determined by using a hydrometer (Rand 2003). According to Adewumi, the API gravity can be calculated from the density of the petroleum fluid and this method is presented in Equation (4.46) to (4.49). The API gravity are usually defined at standard conditions ( $P_{stc}=14.7$  psia and  $T_{stc}=60^{\circ}\text{F}$ ).

The Peng Robinson EOS is used to calculate the liquid density, see Equation (4.46) and (4.47). Where,  $Z_{oil}$  is calculated with the procedure describe in Section 4.4.4 and  $MW_i$  is the molecular weight of component  $i$  in the petroleum fluid. The molecular weight for the fluids used in this project is presented in Section 0. The Peng-Robinson EOS provides fair estimates for vapour and liquid densities as long as we are dealing with natural gas and condensate systems (Adewumi).

$$MW_{oil} = \sum_{i=1}^N x_i MW_i \quad (4.46)$$

$$\rho_{oil} = \frac{P_{stc}}{RT_{stc}} \left( \frac{MW_{oil}}{Z_{oil}} \right) \quad (4.47)$$

$$SG = \frac{\rho_{oil}}{\rho_{water}} \quad (4.48)$$

$$^{\circ}API = \frac{141.5}{SG} - 131.5 \quad (4.49)$$

According to Mian (2002), the API gravity of crude oils varies from  $5^{\circ}$  to  $55^{\circ}$ . Average crude oils have a  $25^{\circ}$  to  $35^{\circ}$  range. Light oils are  $35^{\circ}$  to  $45^{\circ}$  and heavy oils are below  $25^{\circ}$ . The lighter crudes (higher API gravity) receive a higher price as compared to the heavier crude. This is because the lighter crudes tend to have more gasoline by volume than the heavier crudes that have proportionately more gas-oil (diesel) and residue cracking stock.

According to E24 AS the North Sea oil price was approximately 50 dollars per barrel for the first quarter of 2009. The °API adjustment collected from Mian (2002) is added to this price and Table 5 presents the crude oil prices as a function of API gravity

**Table 5: Crude oil price as a function of API gravity.**

°API	Price in dollars per barrel
50	49.625
45	50
40	50
30	48.5

Equation (4.50) presents a method for calculating the income from the crude oil sale. Where,  $I$  is the income [\$/s],  $F_{L,3}$  is the liquid outlet flow from the third separator [kg mol/s] and  $c_{mb}=6.29$  is a conversion factor from barrel to  $m^3$ . The MATLAB function *interp1* is used to implement the function  $Price(^{\circ}API)$ .

$$I = \frac{F_{L,3} MW_{oil} c_{mb}}{\rho_{oil}} \cdot Price(^{\circ}API) \quad (4.50)$$

## 5 Optimizing separator pressures (without compressors)

The income from the crude oil sale is maximised for a process with three separators in series. The process is the same as in Section 4.5 and the pressure in the first and second stage separator is used as control variables.

$$\begin{aligned} & \max_{p_{s1}, p_{s2}}(I) \\ & \text{subject to} \\ & 25 \leq p_{s1} \leq 45 \\ & 4 \leq p_{s2} \leq 18 \end{aligned} \tag{5.1}$$

The optimization problem, see Equation (5.1), is solved by brute force optimization. Where,  $p_{s1}$  is the pressure [bar] in the first stage separator,  $p_{s2}$  is the pressure [bar] in the second stage separator and  $I$  is the income from crude oil sale. In brute force optimizing all possible solutions is tested and the method is therefore very slow. Brute force optimization is easy to implement and the optimum of the points tested will be found.

The inequality constraints have both physical and implementation reasons. Breaking the maximum pressure will lead to an explosion in the separator and the compressor system cannot handle pressure lower than the minimum. The vapour liquid equilibrium calculation fails if the process operates in a single phase region. This happens if the pressure reduction between the first and second stage separator is small. The inequality constraints limit the number of possible solutions and therefore make brute force optimization possible.

Figure 10 presents the pseudocode for brute force optimization. The resolution for the pressure is set to 0.1 bars and this gives 201 and 141 possible operation points for the first and second stage separator. The objective function must therefore be calculated 28341 times.

```
 $p_{s1} = [25 \ 25.1 \ \dots \ 45]$ 
 $p_{s2} = [4 \ 4.1 \ \dots \ 18]$ 
 $I_{opt} = 0$ 
for  $j = 1 : \text{size}(p_{s1})$ 
  for  $k = 1 : \text{size}(p_{s2})$ 
    calculate  $I = f(p_{s1}(j), p_{s2}(k))$ 
    if  $I > I_{opt}$ 
       $j_{opt} = j, k_{opt} = k, I_{opt} = I$ 
    end
  end
end
end
```

Figure 10: Pseudocode for brute force optimization.

The brute force optimization method is used to calculate the optimum for three different reservoir fluids. The composition of the reservoir fluids is presented in Section 10.2 and for all three fluids a flow rate of 2791 [kmol/h] is used.

In Figure 11 to Figure 13 the result of this optimization is presented. The black circle is the operation point for the current control system. The white circle is the optimum operation point found by the brute force optimization. In these figures dark red represents the highest income and the numbers beside the colourbar show the income in dollars per second.

The optimization problem appears to be convex and the nonlinear optimization methods in MATLAB will therefore find the global optimum. This will give a huge time reduction compared to using brute force optimization. However, the brute force optimization method is fast enough for testing. The brute force optimization method uses 7 minutes to solve the problem.

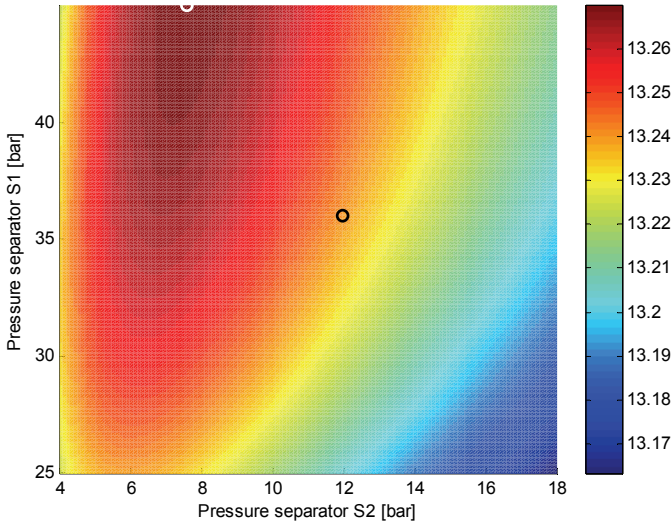


Figure 11: Graphical representation of income as a function of the pressure in separator S1 and S2 for fluid 1.

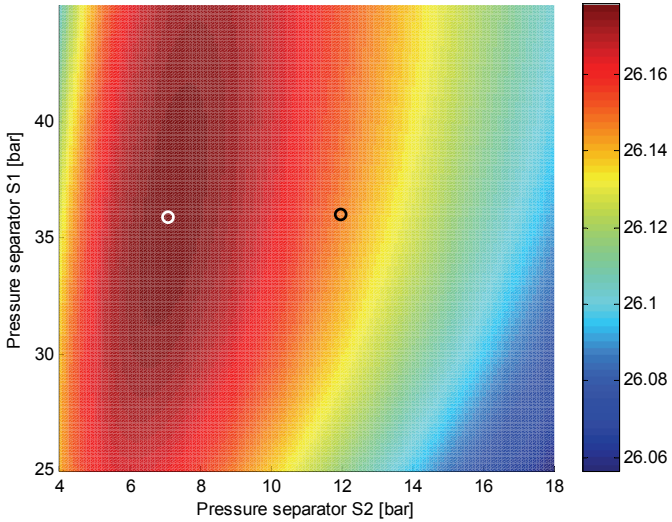


Figure 12: Graphical representation of income as a function of the pressure in separator S1 and S2 for fluid 2.

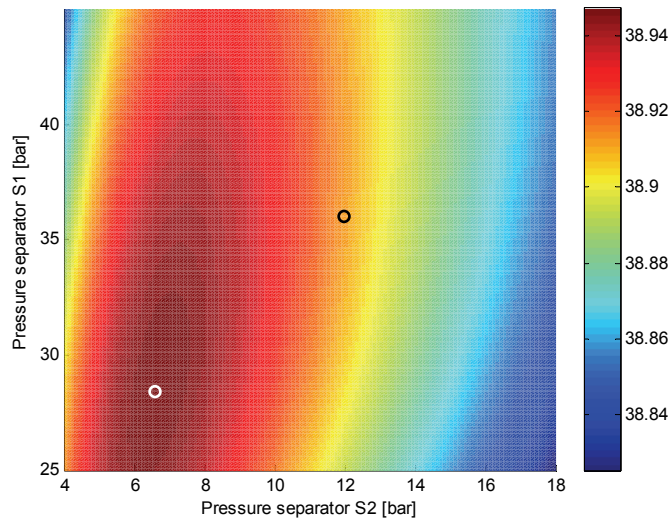


Figure 13: Graphical representation of income as a function of the pressure in separator S1 and S2 for fluid 3.

The optimum operation point changes when the composition of the reservoir fluid is changed and the current operation point is far from the optimum for the three fluids tested. It is possible that the new set-points are infeasible. This is because the compressor model is not incorporated into this model.

Table 6 compares the income from the crude oil sale when the old and new control structure is used. The new control structure gave an average increase in income of 0.14 %. This number is quite small but the average increase in income for a year is one million dollar. It is reasonable to assume that the increase in income will be lower when the compressor model is incorporated.

Bahadori, Vuthaluru, & Mokhatab (2008) performed similar optimization for a gas oil separation process with four separators and the same flow rate. They found the increase in income to be 3600 [\$/day] and 3000 [\$/day] for the summer and winter seasons respectively.

Table 6: Comparison between old and new control method.

	Income old set-point [\$/s]	Income new set-point [\$/s]	Increase [%]	Increase [\$/day]
<b>Fluid 1</b>	13.24	13.27	0.23	2627
<b>Fluid 2</b>	26.15	26.18	0.12	2712
<b>Fluid 3</b>	38.91	38.95	0.09	3058





## 6 Field processing of natural gas

The gas from the three separators needs to be compressed before it can be piped to the injection system. Figure 14 presents the PI&D for the gas compression and gas oil separation plant. The injection system is omitted from this thesis and it is assumed that the discharge pressure for compressor C2 must be larger than 148 [bar]. Pressure below this value will give an infeasible operation condition for the injection system. The purpose of injection is to maintain overall and hydrostatic reservoir pressure and force the oil toward the production wells, (Devold, 2006).

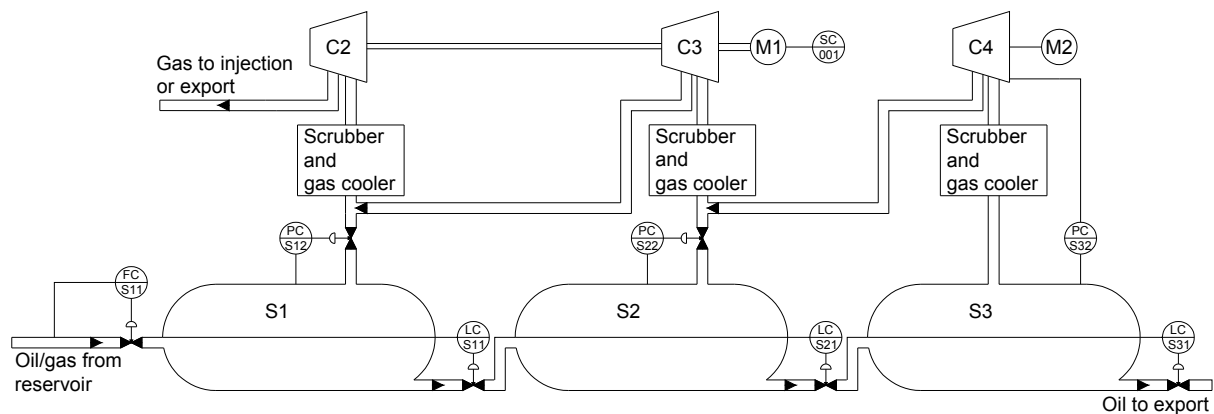


Figure 14: PI&D for the gas compression and gas oil separation plant.

The gas from the separator and the earlier compressor is quite hot and needs to be cooled down before it can be compressed. The cooling increases the gas density and the compressor can therefore have less physical size. On Snorre A the gas temperature from the separator is approximately 70 °C and the gas from the earlier compressor is even hotter, approximately 123 °C. The gas has to be cooled down to approximately 30 °C before it reaches the next compressor. When the gas is cooled down, some of the heavy hydrocarbons will begin to condense. Therefore a scrubber must be placed after the heat exchanger to remove the liquid.

Liquids and solids will reduce the compressors expected lifetime and in more extreme cases instantly destroy the compressor. The scrubber is a large vertical cylinder where the gas enters near the bottom and is discharged at the top of the cylinder. The reduced gas speed and a vane pack in the cylinder lets the oil droplets fall to the bottom. This condensate, the oil droplets, is then pumped back to the inlet of the separator. This thesis, however, assumes that no liquid is pumped back to the separator.

Compressor C4 is driven by a fixed speed electric motor and is fitted with inlet guide vanes. Pressure in separator S3 is controlled by manipulating the inlet guide vane angle for compressor C4. The pressure in separator S1 and S2 is controlled by manipulating the gas valve opening.

Compressor C2 and C3 are multistage variable speed centrifugal compressors and they are connected to the same shaft. The shaft is connected to a variable speed gas turbine and the two compressors will therefore have the same speed.

The gas turbine is designed to operate at speed around 3428 rpm and is connected to a gear box with a ratio of 3.9189. The nominal shaft speed is  $N_o=13434$  rpm. The numbers seen in Figure 17 and Figure 18 is the relative compressor speed  $N_c$ . Where  $N_c=N/N_o$  and  $N$  is the shaft speed. The relative compressor speed can be adjusted from 0.9 to 1.05. The gas turbine speed is controlled such that the gas valve opening for separator S2 is 95% open.

A secondary pressure control system is also fitted to the three separators. The set-points for this system is 0.5 [bar] higher than the set-points for the primary pressure control system. The gas from this system will be burned at the torch and the use of this system should therefore be minimized. The secondary pressure control system is not implemented in this thesis.

## **6.1 Compressors**

The purpose of the compressor is to increase the pressure of gas from one level to another. Depending on the volume flow and pressure ratio different compressor types are used. According to Forsthofer (2005), some different compressor types are: rotary lobe, rotary screw, centrifugal single stage, centrifugal multi-stage and axial compressor.

In offshore oil and gas production the centrifugal multi-stage compressor is the most common, and this compressor is used in this project. In Figure 15 a principle drawing of a centrifugal multi-stage compressor is shown. The compressor consists of mainly three parts: impeller, diffuser and volute/collector.

In a centrifugal compressor the energy of the gas is increased in the impeller. Here mechanical energy from the shaft is used to increase the tangential velocity in the gas. The increase in the tangential velocity will give an increase in pressure. In the diffuser and the volute the tangential velocity will decrease and this gives additional pressure rise. According to (Cohen, Saravanamuttoo, & Rogers, 1996), it is common to design compressors so that about half the pressure rise occurs in the impeller and the other half in the diffuser.

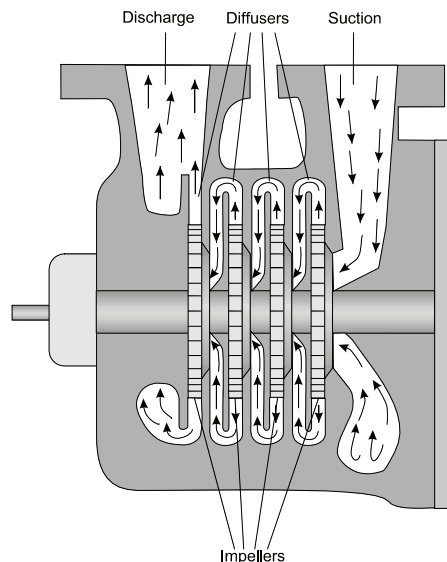


Figure 15: principle drawing of a centrifugal multi-stage compressor (Picture from Siemens).

According to Gravdahl & Egeland (1999), the useful range of operation of turbo-compressors, both axial and centrifugal, is limited, by choking at high mass flows when sonic velocity is reached in some component, and at low mass flows by the onset of two instabilities known as surge and rotating stall. According to Helvoirt (2007), surge not only limits compressor performance and efficiency but can also damage the compressor and auxiliaries due to the large thermal and mechanical loads involved.

Operation in the unstable regime is possible if some advanced control strategy, such as closed coupled valve or drive torque actuation, is used. For more information on these control methods, consult (Bøhagen, 2007) for drive torque and (Gravdahl & Egeland, 1999) for closed coupled valve. These two methods need more research before they can be widely implemented in the industry. Therefore this project will use the traditionally method to prevent surge and rotating stall. This is done with a recycle valve that limits the compressor to operate in the stable regime.

In Figure 16 the compressor characteristics for compressor C2 is given. The four blue lines represent different impeller speeds, where the lines numbered 1, 2, 3 and 4 have the impeller speed 12090, 12762, 13434 and 14105 [rpm] respectively. From the figure we can see that an increase in impeller speed gives an increase in the pressure ratio for the same mass flow. Pressure ratio is defined as the discharge pressure divided on the inlet pressure.

The red dashed line is the surge line and the compressor must operate to the right of this line to be in the stable regime. When the compressor operates in this regime, a reduction in the outlet mass flow will lead to an increase in the pressure ratio and therefore also an increase in the discharge pressure. The increase in discharge pressure will increase the mass flow and the compressor system will converge to a new equilibrium closer to the surge line.

If the reduction in mass flow is large and the surge line is crossed, the change in pressure ratio will be proportional with the change in mass flow. The compressor system will then

become unstable, because a reduction in mass flow leads to a reduction in pressure ratio, which in turn gives a reduction in mass flow.

In this project surge and rotating stall is avoided by using a recycle valve, see Figure 25 on page 52 for block diagram. The compressor is fitted with an anti surge controller that opens the recycle valve when the process crosses the surge control line. When the recycle valve is open the fluid is fed back to the compressor intake and the mass flow is therefore increased.

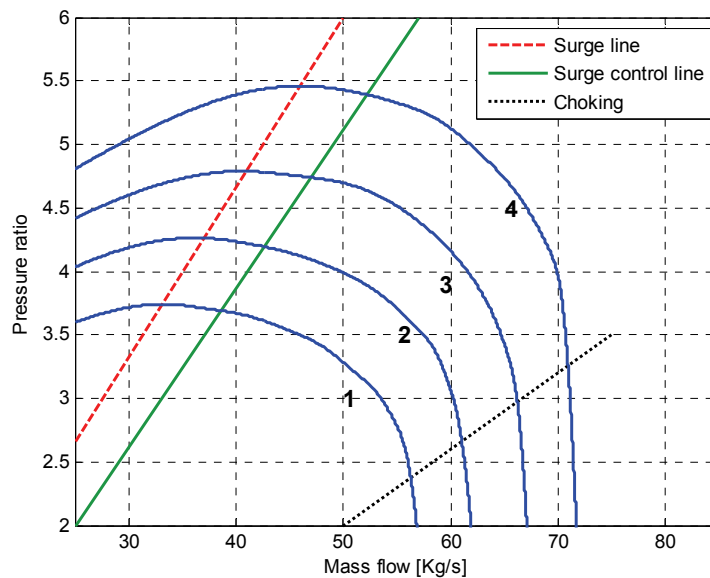


Figure 16: Compressor characteristics with limitation.

The disadvantage with using this anti surge method is that the fluid that passes through the recycle valve must be compressed in the compressor a second time and therefore the overall efficiency of the compressor is reduced.

To the right of the black dotted line in Figure 16 the effect of choking, also known as stonewall, is dominant. Choking occurs when sonic velocity is reached in some component. This phenomenon only limits the range of operations and does not give an unstable regime such as surge and rotating stall.

## 6.2 Isentropic head and isentropic efficiency

The preferred gas compression method with regard to energy consumption is isothermal compression. In isothermal compression the temperature of the gas stays constant. When gas is compressed the temperature increases and the gas must therefore be cooled while it is compressed. According to the Purdue Research Foundation (2006), this is extremely difficult to achieve because, for practical compression machines, the area available for heat transfer is very small and the compression process occurs very quickly.

Since isothermal compression is almost impossible to implement, the compression process is compared against an isentropic compression process. In an isentropic process the entropy is constant. By assuming constant entropy it is possible to establish a relation between temperature and pressure for an ideal gas with constant specific heats, see Equation (6.1). Equation (6.1) was derived in the book White (2008) chapter nine.

$$\frac{p_2}{p_1} = \left( \frac{T_2}{T_1} \right)^{\frac{k}{k-1}} \quad (6.1)$$

According to Hanlon (2001), isentropic head is defined as the energy per mass unit accumulated by the fluid subsequent to a reversible (and thus isentropic) adiabatic transformation between states 1 and 2. An adiabatic process is a process where no heat is transferred to or from the working fluid. According to Philip (1999), the isentropic head  $H_i$  associated with compressing the gas from the inlet pressure  $p_1$  to the discharge pressure  $p_2$ , takes the form:

$$H_i = \frac{k}{k-1} Z R_w T_1 \left( \left( \frac{p_2}{p_1} \right)^{\frac{k-1}{k}} - 1 \right) \quad (6.2)$$

The mean of the specific heats and the compressibility factor is used since these values change slightly from the inlet to the discharge. Philip (1999) defined the isentropic efficiency  $\eta_i$  as:

$$\eta_i = \frac{m_c H_i}{P} \quad (6.3)$$

Where T is the temperature [K], p is the pressure [Pa],  $R_w$  is the characteristic gas constant [J/kgK], k is the specific heats, Z is the compressibility factor, P is the power [W] used by the compressor,  $m_c$  is the mass flow [kg/s] through the compressor and the subscript 1 is taken to refer to the inlet, while 2 refers to the discharge.

In Figure 17 the pressure ratio and isentropic efficiency for compressor C2 is presented. The isentropic efficiency is calculated by using Equation (6.2) and (6.3). The isentropic efficiency presents some interesting properties for compressor C2.

At the surge line the isentropic efficiency is quite low and proportional with the mass flow. Therefore the benefits of implementing an active surge controller will be small. The peak isentropic efficiency of 74% is less than what is typical for centrifugal compressors. According to Philip (1999) the typical design point isentropic efficiency for a centrifugal compressor is in the high 70s %. The most of the compressor characteristic has the isentropic efficiency between 70 to 74% and there is therefore little to gain by changing the operation point.

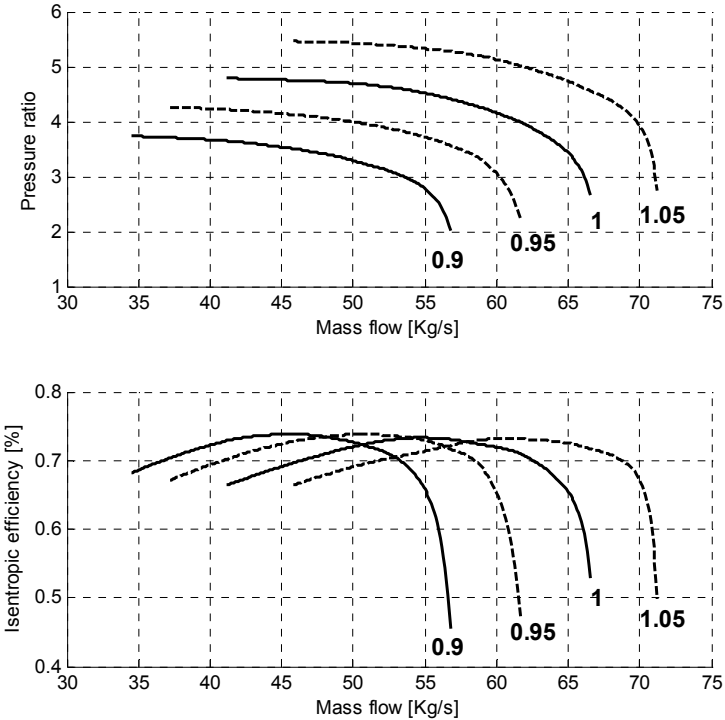


Figure 17: Pressure ratio and isentropic efficiency for compressor C2.

One weakness with using isentropic efficiency is that compressors with different pressure ratios cannot be compared to each other. Therefore it is quite common to use polytropic efficiency in the compressor literature. According to Philip (1999) the isentropic efficiency is between about 2% and 7% less than the polytropic efficiency. In this project there is no need to compare compressors with different pressure ratio and therefore isentropic efficiency is used. More information on polytropic efficiency can be found in Dixon & Eng (1998), Hanlon (2001) or Philip (1999).

### 6.3 Pressure control in separator S1 and S2

The pressure in separator S1 and S2 is controlled by a pressure controller. The controllers are: PC-S12 for the first stage separator (S1) and PC-S22 for the second stage separator (S2). The controller measures the gas pressure and regulates the amount of gas leaving the separator through a choke valve, see Figure 14.

The valve is modelled as in the book Egeland & Gravdahl (2002) chapter 13, see Equation (6.4). Where  $p_i$  is the pressure [Pa] in the separator,  $p_d$  is the pressure [Pa] after the choke valve,  $V$  is the valve constant,  $m$  is the outlet gas mass flow [kg/s] from the separator and  $u$  is the valve opening. The valve cannot be more than fully open or less than completely closed and the valve opening must therefore be between zero and one.

$$m = \begin{cases} uV\sqrt{p_i - p_d} & \text{if } p_i \geq p_d \\ -uV\sqrt{p_d - p_i} & \text{if } p_i < p_d \end{cases} \quad (6.4)$$

The valve constant is found by solving Equation (6.4) with respect on  $V$  when the conditions presented in Table 7 are used. This gives a valve constant of 0.33 for the valve connected to separator S1 and 0.025 for the second valve. The valve opening is found by rearranging Equation (6.4) to Equation (6.5)

$$u = \begin{cases} \frac{m}{V\sqrt{p_i - p_d}} & \text{if } p_i \geq p_d \\ -\frac{m}{V\sqrt{p_d - p_i}} & \text{if } p_i < p_d \end{cases} \quad (6.5)$$

Table 7: Values used for calculating the valve constant.

	Separator S1	Separator S2	Description
$p_i$	$36 \cdot 10^5$ [Pa]	$12 \cdot 10^5$ [Pa]	Pressure in separator
$p_d$	$35.7 \cdot 10^5$ [Pa]	$11.7 \cdot 10^5$ [Pa]	Pressure after the gas valve
$m$	55 [Kg/s]	4 [Kg/s]	Outlet gas mass flow from the separator
$u$	0.95	0.95	Valve opening





## 7 Compressor modelling

Compressor characteristics are a common way to represent compressor performance. Figure 18 presents the design pressure ratio and power consumption for compressor C2 and compressor C3. These four graphs must be implemented in the compressor simulation model and this can be done in many different ways. Some of the different methods used for implementation are polynomial approximation, physical modelling and dimensionless parameters. All the methods have different advantages and disadvantages and a short description of the methods will be given in the following subsections.

The compression plant has two multistage variable speed centrifugal compressors and the compressor characteristics for these two compressors are presented in Figure 18. Where the black x-marks are points obtained from Aker Engineering a.s (1996a), the red line is the surge line, the blue x-marks are an expansion of the compressor characteristics, the dotted line is a linear interpolation between the x-marks and the numbers beside the lines show the relative compressor speed. The inlet conditions for the compressor characteristics are presented in Table 14.

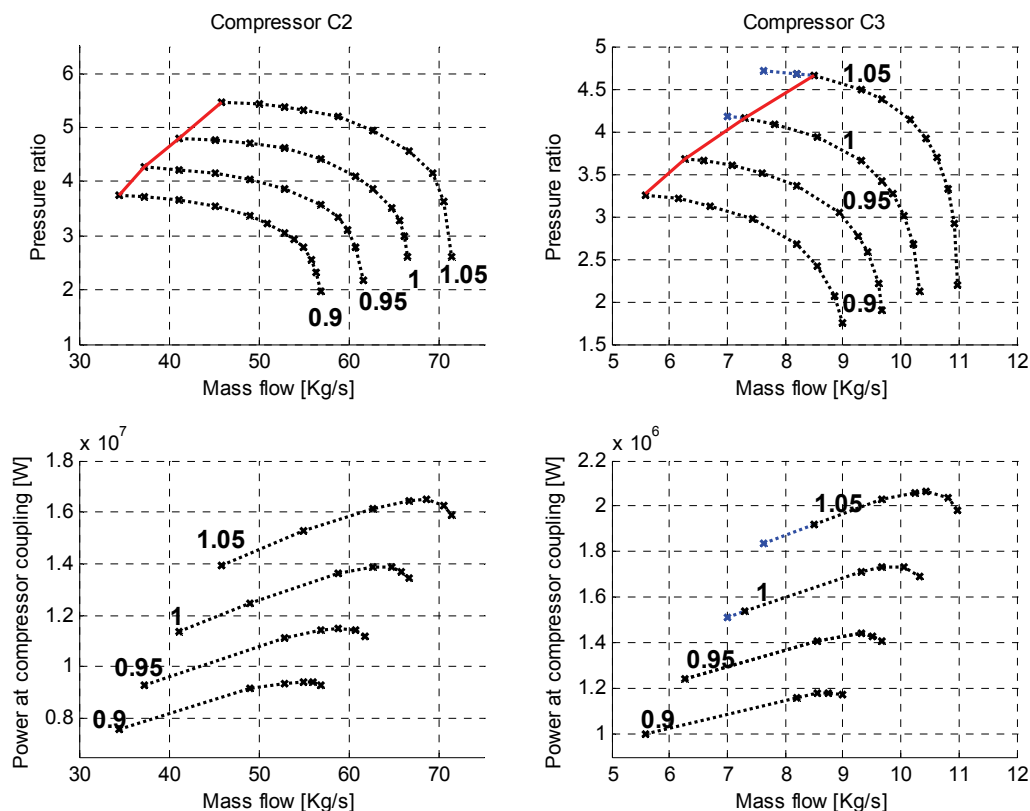


Figure 18: Compressor characteristic for compressor C2 and compressor C3.

## 7.1 Polynomial approximation

The pressure ratio can be estimated with a polynomial and this approach is used by Bøhagen (2007), Egeland & Gravdahl (2002), Willems (2000) and Helvoirt (2007). Equation (7.1) shows the polynomial approximation proposed by Willems (2000) also used by Bøhagen (2007). The unknown coefficients  $c_{i,j}$  can be found with linear least-squares and this is described in Section 10.1.

$$p_r(m, S) = c_3(S)m^3 + c_2(S)m^2 + c_0(S) \quad (7.1)$$

$$c_i(S) = c_{i,2}m^2 + c_{i,1}m + c_{i,0}$$

Figure 19 presents the polynomial approximation of the pressure ratio for compressor C2. The x-marks are the points collected from the datasheet supplied by the manufacturer. The dashed lines is a shape-preserving piecewise cubic interpolation of the x-marked points. This line is calculated with a fixed step size of 0.1 kg/s in the x-axis. The solid line is the polynomial approximation where all the points from the dashed lines are used.

This figure illustrates that the polynomial approximation proposed by Bøhagen (2007) is inaccurate when the whole pressure ratio curve is approximated. Bøhagen used a single stage centrifugal compressor. This compressor has a smoother curve and the derivative is smaller at high mass flow. Figure 19 shows that the polynomial approximation fails to estimate the points near the stonewall.

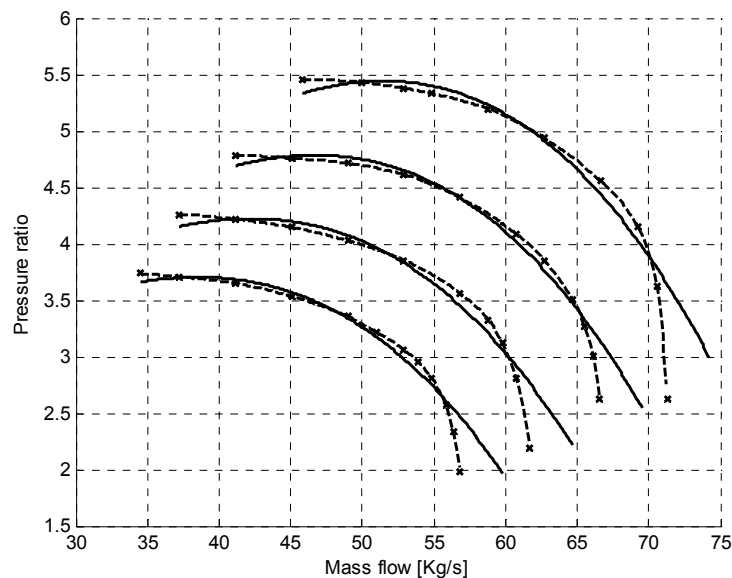


Figure 19: Polynomial approximation of the pressure ratio 1.

The solid line in Figure 20 is a polynomial approximation of the pressure ratio for compressor C2. In Figure 20 the dashed line to the left of the circle is used in the polynomial approximation.

This approach gives a tight fit between the solid and dashed line for points placed left to the circle. Bøhagen used this polynomial approximation in the thesis “Active surge control of centrifugal compressor system”. The part of the dashed line that is omitted is insignificant for active surge control system. This is because the compressor system is stable and this region is far from the surge line. Figure 17 shows that the isentropic efficiency is quite high for this region and it is therefore likely that the compressor system will operate in this region.

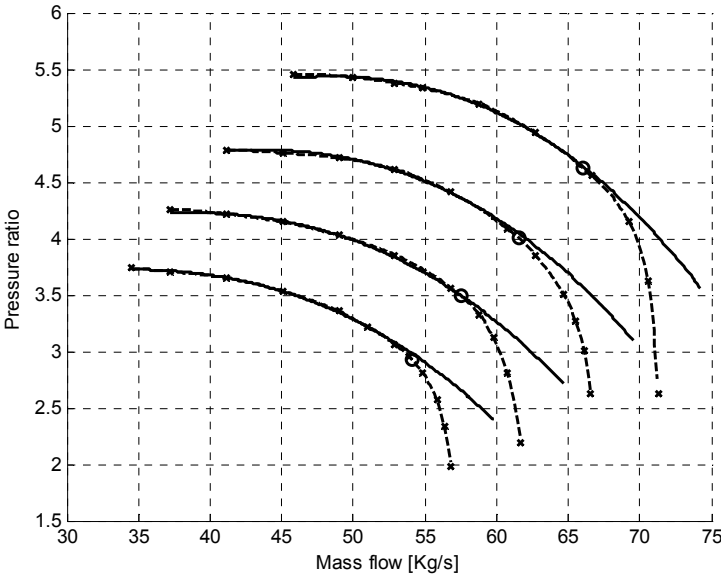


Figure 20: Polynomial approximation of the pressure ratio 2.

### 7.1.1 Polynomial + nonlinear term approximation of the pressure ratio

An alternative approach is to approximate the pressure ratio for the four speed lines and then use linear interpolation to estimate the pressure ratio for the other speed.

High order polynomials can be highly oscillatory and the polynomial order should therefore be held as low as possible. Equation (7.2) presents a method for estimating the pressure ratio, where  $c_{1,i}$  to  $c_{7,i}$  are the unknown parameters and the subscript  $i$  is used to separate the four different speed lines from the manufacture. This method consists of a cubic polynomial approximation and a nonlinear term. The unknown coefficients cannot be calculated with linear least-squares since the method contains a nonlinear term.

A cubic polynomial approximation gives a tight fit between the model and the measurements, when the points near the stonewall area of the measured characteristics

were not used. This method will therefore use a cubic polynomial approximation for this part. For the points near the stonewall area a nonlinear term will be added to improve accuracy.

$$\begin{aligned}
 & \text{if } c_{5,i} > m \\
 & \quad \widehat{p}_{r,i} = c_{1,i}m^3 + c_{2,i}m^2 + c_{3,i}m + c_{4,i} \\
 & \text{else} \\
 & \quad \widehat{p}_{r,i} = c_{1,i}m^3 + c_{2,i}m^2 + c_{3,i}m + c_{4,i} + c_{6,i}(m - c_{5,i})^{c_{7,i}} \\
 & \text{end}
 \end{aligned} \tag{7.2}$$

This curve fitting procedure consists of two steps:

1. The unknown parameters  $c_{5,i}$  to  $c_{7,i}$  are set to zero and the remaining term is then a cubic polynomial. The coefficients of this polynomial are found with the MATLAB command *polyfit*.
2. The remaining unknown parameters  $c_{5,i}$  to  $c_{7,i}$  are calculated with the MATLAB command *fminsearch*. *Fminsearch* searches for the minimum of Equation (7.3), where  $p_{r,i}$  is the shape-preserving piecewise cubic interpolation of a constant speed line from the manufacture.

$$\min_c \left\| p_{r,i} - \widehat{p}_{r,i} \right\|^2 \tag{7.3}$$

Figure 21 presents a comparison between the shape-preserving piecewise cubic interpolation (dashed black line) and the polynomial + nonlinear term approximation (blue line). The blue line nearest the lower left corner has a relative compressor speed of 0.85 and the speed is increased with 0.01 for each new blue line. The preserving piecewise cubic interpolation line and the blue line for the same speed fits almost perfectly and this method seems to give good results between the speed lines too.

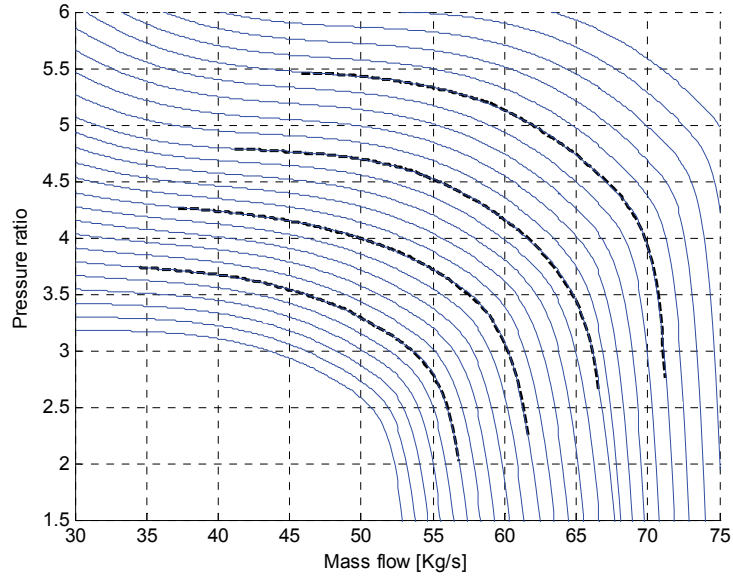


Figure 21: Polynomial + nonlinear term approximation of the pressure ratio.

### 7.1.2 Polynomial + nonlinear term approximation of the power consumption.

The approach used above is used to approximate the power consumption. Equation (7.4) presents the approximation of the power consumption for a constant speed. Figure 22 shows the comparison between the measured power consumption (dashed black line) and the polynomial + nonlinear term approximation (blue line).

$$\begin{aligned}
 & f c_{3,i} > m \\
 & \hat{P}_i = c_{1,i} m + c_{2,i} \\
 & \text{else} \\
 & \hat{P}_i = c_{1,i} m + c_{2,i} + c_{4,i} (m - c_{3,i})^{c_{5,i}}
 \end{aligned} \tag{7.4}$$

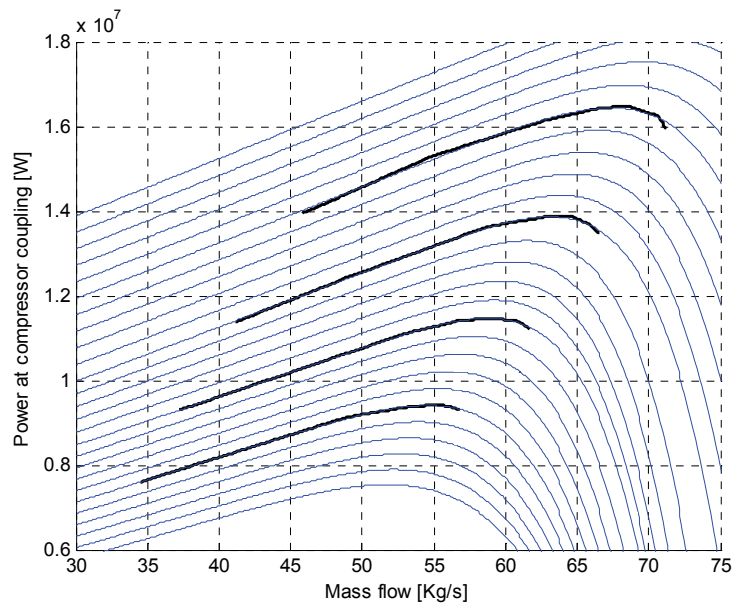


Figure 22: Polynomial + nonlinear term approximation of the power consumption.

### 7.1.3 Conclusion

Polynomial plus nonlinear term approximation gives a good approximation of the compressor characteristics for the design inlet conditions. A change in the separator pressure will influence the inlet pressure to the compressor. Small changes in the molecular weight will also accrue when the reservoir fluid composition changes. The compression system will therefore operate in off-design operation points. According to Hanlon (2001), off-design operation of a compressor can dramatically affect the pressure ratio and power consumption.

Polynomial plus nonlinear term approximation can therefore not be used since this method gives the same compressor characteristics for all inlet conditions.

## 7.2 Physical modelling

In physical modelling first principal of physics are used to derive a model for the compressor system. This approach was used by Gravdahl & Egeland (1999) and parts of this model will be used here. This model is a dynamic model for a variable speed centrifugal compressor and is based on compressor geometry and energy considerations.

When the model was derived, it was assumed that compression process is isentropic and that the gas has constant specific heat. With these two assumptions the discharge pressure can be calculated as seen in Equation (7.5).

$$p_{d,c} = \left( 1 + \frac{\eta_i(m, U_1) \Delta h_{0c,ideal}}{T_{i,c} c_p} \right)^{\frac{k}{k-1}} p_{i,c} \quad (7.5)$$

Where  $\eta_i(m, U_1)$  is the isentropic efficiency,  $\Delta h_{0c,ideal}$  is the ideal specific enthalpy delivered to the fluid,  $k$  is the ratio of specific heats and  $c_p$  is the specific heat capacity at constant pressure.

The slip factor  $\sigma$  depends largely on the number of impeller blades, but also on the passage geometry, the impeller eye tip exit diameter ratio and mass flow rate, (Gravdahl & Egeland, 1999). With a constant slip factor and a radially vaned impeller the ideal specific enthalpy delivered to the fluid can be expressed as:

$$\Delta h_{0c,ideal} = \sigma U_2^2 \quad (7.6)$$

The maximum pressure ratio, for a constant speed, in Equation (7.5) occurs when the isentropic efficiency is at the maximum. This is not the case for compressor C2, see Figure 17, and this indicates that the slip factor is not constant.

$$\eta_i(m, U_1) = \frac{\Delta h_{0c,ideal}}{\Delta h_{0c,ideal} + \Delta h_{loss1}} - \Delta h_{loss2} \quad (7.7)$$

In Equation (7.7) the isentropic efficiency of the compressor is presented, where  $\Delta h_{loss1}$  is the sum of incidence and frictional losses in the impeller and diffuser.  $\Delta h_{loss2}$  represents other losses. In the work of (Gravdahl & Egeland, 1999) model for the  $\Delta h_{loss1}$  is presented and  $\Delta h_{loss2}$  is assumed constant.

The compressors power consumption is:

$$P_c = \sigma(D_2 N)^2 |m_c| \quad (7.8)$$

Where  $D_2$  is the diameter at the impeller tip and  $N$  is the number of revolutions per second. The power consumption for a constant speed as a function of mass flow is a straight line. Figure 18 shows that the physical model proposed by Gravdahl & Egeland (1999) cannot be used to accurately model the power consumption for compressor C2 and C3. This is because the power consumption for a constant speed as a function of mass flow is not a straight line.

Common practice in the literature was and still is to use an approximation of the pressure rise characteristic (Helvoirt 2007). This is because physical modelling gives many unknown parameters that must be estimated. The model is nonlinear and this estimation is therefore difficult. Physical modelling will not be used in this thesis.



### 7.3 Dimensionless parameters

According to Nørstebø (2008) the compressor characteristics may be specified by equations of different dimensionless parameters. These equations will not be dependent on inlet pressure, temperature, molecular weight or compressor speed. Nørstebø proposed the dimensionless factors presented in Equation (7.9) to (7.11). The exponents of  $T_i$ ,  $MW_c$  and  $S$  can be modified in order to fit better with the actual compressor system.

Flow coefficient:

$$\varphi_c = \Upsilon \frac{m\sqrt{T_i}}{p_i\sqrt{MW}S^1} \quad (7.9)$$

Pressure coefficient:

$$\omega_c = \frac{p_d}{p_i S^2} \quad (7.10)$$

Power coefficient:

$$\psi_c = \frac{P\sqrt{MW}}{p_i\sqrt{T_i}S^3} \quad (7.11)$$

Where  $m$  is the mass flow,  $T_i$  is the inlet temperature,  $MW$  is the molecule weight,  $p_d$  is the discharge pressure,  $p_i$  is the inlet pressure,  $S$  is the relative compressor speed,  $P$  is the power consumption and  $\Upsilon$  is used to scale the value properly. The scaling improves the numerical properties for the pressure and power coefficient approximation.

The compressor characteristic from the manufacture is a function of mass flow and relative compressor speed. Since the compressor characteristic from the manufacture is not a function of temperature and molecular weight, the exponents for these to values cannot be tuned.

Figure 23 shows the relationship between flow and pressure coefficients, and between flow and power coefficients. The first column is for compressor C2 and the second column is for compressor C3. In Figure 23 the light grey, grey, dark gray and black lines are the speed lines for the manufacture. The relative compressor speeds are 0.9, 0.95, 1 and 1.05 for these lines.

The exponents of  $S$  are tuned such that the area between these lines are minimised. This minimisation can be done by trial and error or by an optimization algorithm which is presented in Section 7.3.1. This project uses the optimization algorithm presented in Section 7.3.1 and Figure 23 shows the result of this optimization.

The green line in Figure 23 is a third order polynomial approximation of the pressure coefficient. For compressor C2 the flow coefficient data between 1.25 and 2 are used. Compressor C3 has a larger deviation between the four speed lines. The light grey line has a large deviation from the three other lines for flow coefficient data less than 0.63 and these

data are therefore removed. After these data are removed, the flow coefficient data between 0.6 and 0.87 are used for the third order polynomial approximation.

Equation (7.12) presents this method and the unknown coefficients,  $c_{a1}$  to  $c_{a4}$ , are found with the MATLAB command *polyfit*. If the entire flow coefficient data is used the polynomial order must be increased to seven to give a good approximation. High order polynomials can be highly oscillatory and the polynomial order should therefore be as low as possible

$$\hat{\omega}_c = c_{a1}\varphi_c^3 + c_{a2}\varphi_c^2 + c_{a3}\varphi_c + c_{a4} \quad (7.12)$$

The third order polynomial approximation gives a precise estimation of the four speed lines from the manufacture for the flow coefficient data used in the estimation. In Equation (7.13) an alternative method is shown. This method uses the third order polynomial approximation presented above and a nonlinear term. The three unknown coefficients,  $c_{a5}$  to  $c_{a7}$ , can easily be found by trial and error.

Selecting  $c_{a5}$  positive and  $c_{a7}$  greater than three guarantees that the nonlinear term becomes the dominant factor for large mass flow. This ensures that the pressure coefficient continues to decline for flow coefficients data larger than the data used in this approximation. If a high order polynomial is used the opposite can occur and this is clearly unphysical.

The blue line in Figure 23 shows the result of this curve fitting method. The deviation between the blue line and the speed lines from the manufacture is small.

$$\begin{aligned} & \text{if } (\varphi_c < c_{a6}) \\ & \hat{\omega}_c = c_{a1}\varphi_c^3 + c_{a2}\varphi_c^2 + c_{a3}\varphi_c + c_{a4} \\ & \text{else} \\ & \hat{\omega}_c = c_{a1}\varphi_c^3 + c_{a2}\varphi_c^2 + c_{a3}\varphi_c + c_{a4} - (c_{a5}(\varphi_c - c_{a6}))^{c_{a7}} \end{aligned} \quad (7.13)$$

The red line in Figure 23 is the fifth order polynomial approximation of the power coefficient, see Equation (7.14). The pressure and power coefficients approximation will be used to calculate the discharge pressure and power consumption for compressor C2 and C3.

$$\hat{\psi}_c = c_{b1}\varphi_c^5 + c_{b2}\varphi_c^4 + c_{b3}\varphi_c^3 + c_{b4}\varphi_c^2 + c_{b5}\varphi_c + c_{b6} \quad (7.14)$$

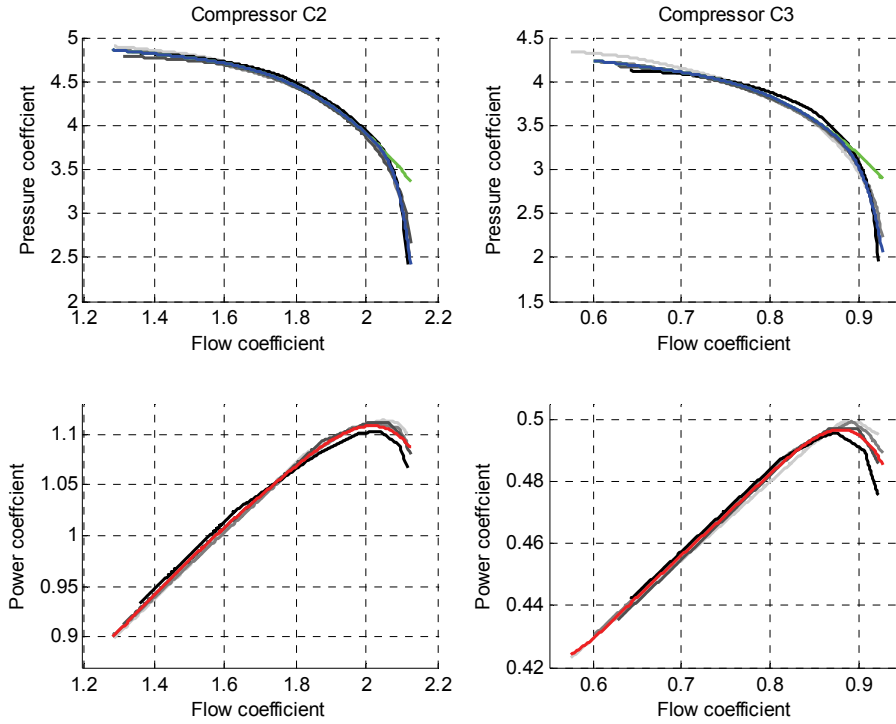


Figure 23: Relationship between flow and pressure coefficient, and between flow and power coefficients.

### 7.3.1 Algorithm for calculating the optimal exponents of S

The calculation of the optimal exponents of S is an unconstrained nonlinear minimization problem and the MATLAB function *fminsearch* is used to find the optimum. *Fminsearch* uses the Nelder-Mead simplex direct search algorithm to find the minimum. This function minimizes the object function with respect on the optimization variables *exs1* to *exs3*

Object function:

1. Calculate Equation (7.15) to (7.17) for  $j=[1,2,3,4]$ , where  $j$  is the speed lines from the manufacture and  $\Upsilon$  is used to scale the value properly. The scaling transformation improves the numerical properties of this algorithm.

$$\varphi_{c,j} = \Upsilon_1 \frac{m_{c,j} \sqrt{T_{i,c}}}{p_{i,c} \sqrt{MW_c} S^{exs1}} \quad (7.15)$$

$$\omega_{c,j} = \frac{P_{r,c,j}}{S^{exs2}} \quad (7.16)$$

$$\psi_{c,j} = \Upsilon_2 \frac{P_{c,j} \sqrt{MW_c}}{p_{i,c} \sqrt{T_{i,c}} S^{exs3}} \quad (7.17)$$

2. Calculate the polynomial in Equation (7.18) which gives the smallest square error compared to Equation (7.15) and (7.16).

$$\omega = P_1\varphi^9 + P_2\varphi^8 \dots + P_9\varphi + P_{10} \quad (7.18)$$

3. Calculate the polynomial in Equation (7.19) which gives the smallest square error compared to Equation (7.15) and (7.17).

$$\psi = P_1\varphi^9 + P_2\varphi^8 \dots + P_9\varphi + P_{10} \quad (7.19)$$

4. Return the sum of the squared errors.

### 7.3.2 Calculation of discharge pressure and power consumption

In the simulation model the inlet conditions, temperature, pressure, molecule weight, relative compressor speed and mass flow are known. The power consumption and discharge pressure can be calculated from these values and this calculation is presented in Equation (7.20)

$$\begin{aligned} \varphi &= \Upsilon \frac{m\sqrt{T_i}}{p_i\sqrt{MW}S^{\text{exs1}}} \\ &\text{if}(\varphi < c_{a6}) \\ &\quad \hat{\omega} = c_{a1}\varphi^3 + c_{a2}\varphi^2 + c_{a3}\varphi + c_{a4} \\ &\quad \text{else} \\ &\quad \hat{\omega} = c_{a1}\varphi^3 + c_{a2}\varphi^2 + c_{a3}\varphi + c_{a4} - (c_{a5}(\varphi - c_{a6}))^{c_{a7}} \\ &\quad \text{end} \\ p_d &= p_i\hat{\omega}S^{\text{exs2}} \\ \hat{\psi}_c &= c_{b1}\varphi^5 + c_{b2}\varphi^4 + c_{b3}\varphi^3 + c_{b4}\varphi^2 + c_{b5}\varphi + c_{b6} \\ P &= \frac{p_i\sqrt{T_i}S^{\text{exs3}}}{\sqrt{MW}}\hat{\psi} \end{aligned} \quad (7.20)$$

Figure 24 presents a comparison between actual compressor characteristics and the dimensionless parameters model, where x-marks are the actual compressor characteristics and the blue line are the dimensionless parameters model. For this operation point the deviation between the model and the actual compressor characteristics is small.

It is assumed that the gas cooler is ideal and the compressor inlet temperature is therefore constant. The compressors inlet pressure and molecular weight is not constant and the dimensionless parameters model should therefore be tested against other operation conditions. Data for other operation conditions were impossible to obtain and it is therefore assumed that the Dimensionless Parameters model gives reasonable result for these operation conditions.

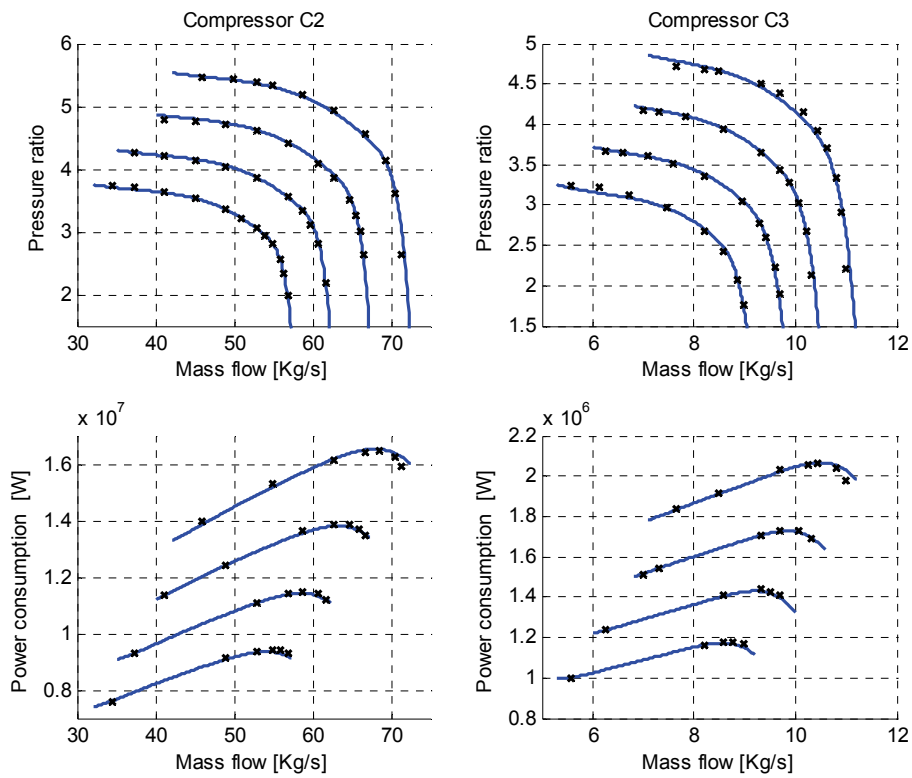


Figure 24: comparison between actual compressor characteristics and dimensionless parameters model.

This thesis will use the Dimensionless Parameters method to model the compressor characteristics. Both physical modelling and Dimensionless Parameters can be used for off-design operation points, but physical modelling is easier to implement and is therefore preferred. Polynomial approximation cannot be used for off-design operation points and is therefore unsuitable for the model derived in this thesis.

## 7.4 Anti-surge control

Surge is avoided in the three compressors by using a recycle valve. The existing control system uses the pressure ratio versus actual volumetric flow scheme to avoid surge. Figure 25 presents the piping and instrument diagram for this control scheme. The anti surge controller used on these three compressors is developed by Siemens and the algorithm for this controller is presented in Siemens (1996). The existing control system is quite complex and another controller will be used to simplify the analysis. The controller used in this project is a PI controller with anti-windup, see Section 10.5 for details.

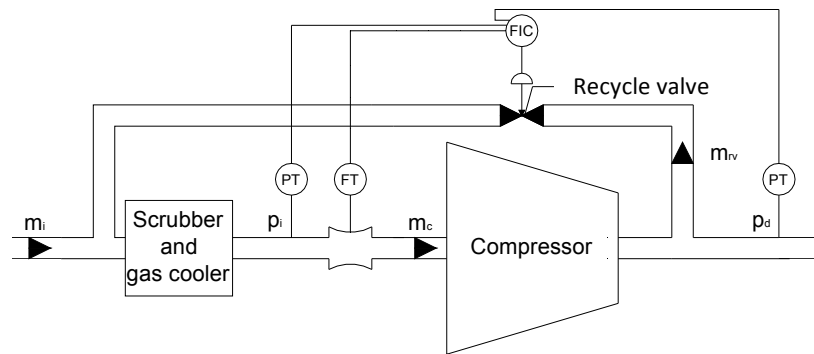


Figure 25: P&ID for compressor C2 and C3.

The input to the PI controller with anti-windup is calculated as seen in Equation (7.21). A positive value of  $E$  will lead to an opening of the recycle valve. The surge avoidance line is found by setting  $E$  to zero.

$$E = c_{as1} + c_{as2} \frac{p_d}{p_i} - \rho m_c \quad (7.21)$$

The minimum possible mass flow through the compressor is calculated by setting  $E$  equal to zero, see Equation (7.22). For compressor C4  $\rho$  is constant and Equation (7.22) can be rearranged to Equation (7.23). The red line in Figure 27 is the surge avoidance line for compressor C4.

$$m_{surge} = \frac{c_{as1}}{\rho} + \frac{c_{as2}}{\rho} p_r \quad (7.22)$$

$$m_{surge} = c_{sa3} + c_{as4} p_r \quad (7.23)$$

The steady state surge controller for compressor C4 is presented in Equation (7.24).

$$\begin{aligned} &\text{if}(m_i < m_{surge}) \\ &\quad m_c = m_{surge} \\ &\text{else} \\ &\quad m_c = m_i \\ &\text{end} \end{aligned} \quad (7.24)$$

The surge control system is designed to operate with small changes in the inlet pressure. The inlet pressure for compressor C2 and C3 is not constant and another surge control method is needed. Dimensionless Parameters are used to model these compressors and an anti-surge controller is incorporated into this model. Equation (7.25) presents the new anti-surge controller, where  $\varphi_{\max}$  is a constant and  $\varphi_c$  is the flow coefficient calculated in Equation (7.9). The new surge control method is more accurate when the inlet conditions changes and it is easier to implement.

$$E = \varphi_{\max} - \varphi_c \tag{7.25}$$

Figure 26 presents the anti-surge controller on compressor C2 and C3. The green and black line is the surge avoidance line. The green line shows the existing control system and the black line shows the new control system.  $\varphi_{\max}$  is selected such that the deviation between the black and green line is minimized. The steady state surge controller for compressor C2 and C3 is presented in Equation (7.24) when  $m_{\text{surge}}$  is replaced with  $\varphi_{\max}$ ,  $m_i$  and  $m_c$  is replaced with  $\varphi_c$ .

The two surge avoidance lines are almost identical for compressor C2 and the replacement of surge controller should therefore have insignificant effects on the simulations.

The compressor characteristics for compressor C3 deviates from other compressor characteristics for a centrifugal compressor. Examples of other compressor characteristics are presented in Figure 1.17 (Gravdahl & Egeland 1999), FIG 8.9aa (Lipták 1995) and Fig C.3 (Helvoirt 2007). All these figures have surge lines with the same shape as the green line in Figure 17(2). Why the surge line for compressor C3 deviates from other surge lines is out of scope for this project. The new surge controller will be used for both compressors.

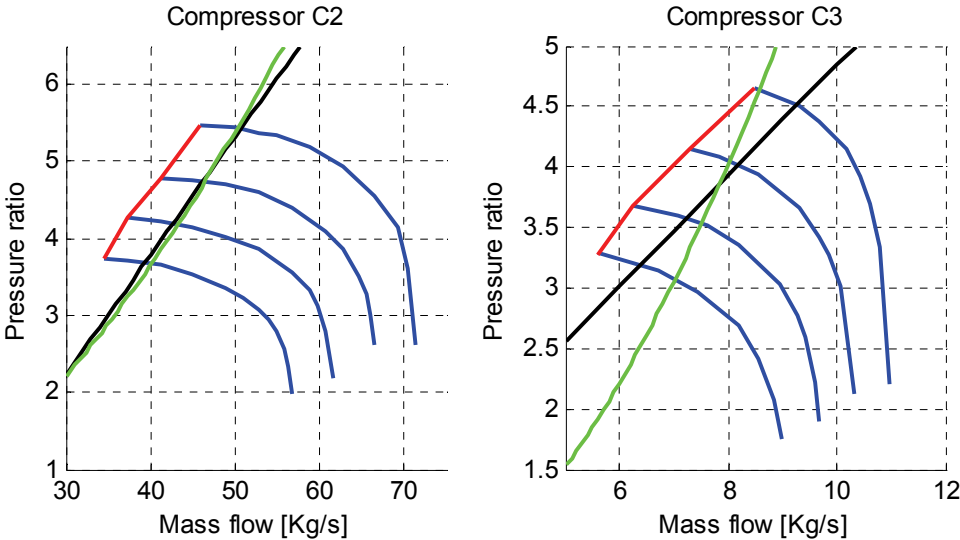


Figure 26: Anti-surge controller on compressor C2 and C3.

## 7.5 Compressor C4

Compressor C4 is a centrifugal compressor with six stages and is driven by a fixed speed electric engine. The compressor is fitted with inlet guide vanes and they are used to control the pressure in separator S3. The inlet pressure and temperature for this compressor is constant. This is because the pressure in separator S3 is constant and it is assumed that the scrubber and gas cooler are ideal components. It is also assumed that the inlet density is constant.

The compressor characteristic seen in Figure 27 is collected from Aker Engineering a.s (1995b) where the black curves represent different angles of the inlet guide vanes. The inlet conditions for this experiment are presented in Table 14.

A straightforward approach is to use the inlet guide vane angle and the mass flow as the input and then use a polynomial approximation to calculate the pressure ratio and power consumption. With this approach a high order polynomial approximation is needed to accurately estimate the pressure ratio and power consumption.

The pressure ratio can be used as the input instead of the inlet guide vane angles. This reduces the order for the polynomial approximation and the power consumption is approximated by Equation (7.26). This makes it possible to select inputs that are infeasible and constraints must therefore be added to the model. Equation (7.28) presents the constraints. Where,  $p_{rmax}$  is the maximum possible pressure ratio for a given mass flow. The blue line in Figure 27 shows the maximum pressure ratio. Linear interpolation is used for the implementation of the function  $p_{rmax}$ .

$$P = c_{p1}m_c + c_{p2}p_r + c_{p3} \quad (7.26)$$

It is assumed that the discharge pressure from compressor C1 must be at least 148 bar. The operation condition that gives the smallest possible pressure ratio for compressor C3 is when compressor C2 and C1 operates at maximum pressure ratio. Equation (7.27) presents the minimum pressure ratio possible for compressor C3.

$$p_{rmin} = \frac{P_{dc1}}{p_{rc2}p_{rc1}p_{sep3}} = \frac{148}{5.6 \cdot 4.8 \cdot 2} = 2.8 \quad (7.27)$$

$$p_{rmin} < p_r < p_{rmax}(m_c) \quad (7.28)$$

The unknown coefficients in Equation (7.26),  $c_{p1}$  to  $c_{p3}$ , is found with linear least squares, see Section 10.1. The endpoints of the five curves were used in this approximation. The error between the actual power consumption, black x-mark, and the estimated power consumption, blue x-mark, is small.



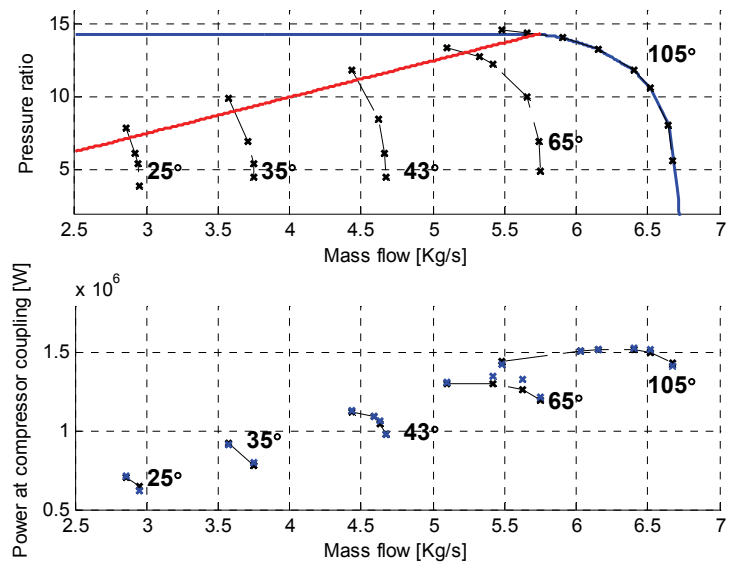


Figure 27: Compressor characteristics for compressor C4.



## 8 Optimizing separator pressures (with compressors)

The gas from the separators must be compressed before it can be sold or injected back to the reservoir. In this thesis it is assumed that the gas is injected back to the reservoir. The model is therefore extended to include the compressors and the process is presented in Figure 14. The optimum operation points found in Section 5 may be infeasible or not optimal when the compression plant is included.

$$\begin{aligned}
 & \max_{p_{s1}, p_{s2}, S, p_{r,c4}} (I - E) \\
 & \text{subject to} \\
 & p_{d,C2} > 148 \\
 & 0.9 < S < 1.05 \\
 & 0 < u_{s1} < 1 \quad 0 < u_{s2} < 1 \\
 & 25 \leq p_{s1} \leq 45 \quad 4 \leq p_{s2} \leq 18 \\
 & 1 < p_{r,C2} \quad 1 < p_{r,C3} \quad 2.8 < p_{r,C4} > 14.3
 \end{aligned} \tag{8.1}$$

$$E = (P_{c2} + P_{c3} + P_{c4}) \text{price}_{el} \tag{8.2}$$

The optimization problem is presented in Equation (8.1). The profit is maximized in the objective function where  $I$  is the income from the crude oil sale and  $E$  is the energy cost for operating the gas turbine and electric engine. It is assumed that the efficiency of the two engines is 100% and that the energy price is  $2.13 \times 10^{-8}$  [\$/Ws]. This corresponds to an energy price of 0.5 [NOK/KWh]. The energy cost is calculated as seen in Equation (8.2) where  $\text{price}_{el}$  is the energy price [\$/Ws].

The profit is calculated as the income from crude oil sale minus the energy cost for operating the gas turbine and electric engine. Additional factors as: implementation cost, taxes and other operation costs will also affect the profit, but these factors are not included in this thesis.

The discharge pressure from compressor C2 must be larger than 148 bar. Lower pressure will give an infeasible operation condition for the injection compressor. The constraint on relative compressor speed is due to limitations in the gas turbine. A negative pressure ratio in compressor C2 or C3 will give a negative pressure for the discharge pressure and this is clearly unphysical. The pressure is reduced before each separator and the pressure ratio in compressor C2 and C3 must therefore be larger than one.

Brute force optimization is used to solve this optimization problem and a pseudocode for this is presented in Section 10.6. The compressor model is dependent of all the four control variables and must therefore be calculated  $N_1 * N_2 * N_3 * N_4 = 100$  million times where  $N_1$ ,  $N_2$ ,  $N_3$  and  $N_4$  is the number of points in the vector  $p_{s1}$ ,  $p_{s2}$ ,  $S$  and  $p_{r,c4}$ , respectively.

The separator model is independent of the relative compressor speed and pressure ratio for compressor C4. It is therefore enough to calculate this model  $N1 \cdot N2 = 3351$  times. This gives a significant reduction to the computation time.

The compressor model has a very small feasible region for some of the first and second stage separator pressure combinations. As a result of this a very small step size for the optimization variables  $S$  and  $P_{r,C4}$  must be used. This increases the number of calculations needed and the brute force optimization method is therefore extremely slow. The computation time for the brute force optimization method presented in Section 10.6 is around 18 hours.

The composition of the reservoir fluids is presented in Section 10.2. The maximum crude oil capacity is limited by the separators and the oil pump. According to Norsk Hydro (2001) the maximum crude oil capacity for Snorre A is 1.31 barrels per second. Table 8 presents the gas and crude oil production for the current control systems. The inlet flow was selected such that the crude oil production is approximately 85% of the maximum.

**Table 8: Gas and crude oil production for four different inlet conditions.**

Experiment	Inlet composition	Inlet flow [kmol/s]	Gas produced [kg/s]	Crude oil produced [b/s]
1	Fluid 1	12000	61.2	1.15
2	Fluid 2	6000	24.1	1.13
3	Fluid 3	4000	12.1	1.12
4	Fluid 4	14000	Infeasible	1.15

The brute force optimization method is used to calculate the optimum for four different experiments, see Table 8. Figure 28 to Figure 31 presents the result of this optimization. Here the black circle is the operation point for the current control system and the white circle is for the new control system. Dark red represents the highest income and the numbers beside the colourbar shows the income in dollars per second. In the dark blue area one of the constraints is violated and operation with this setpoint is therefore impossible.

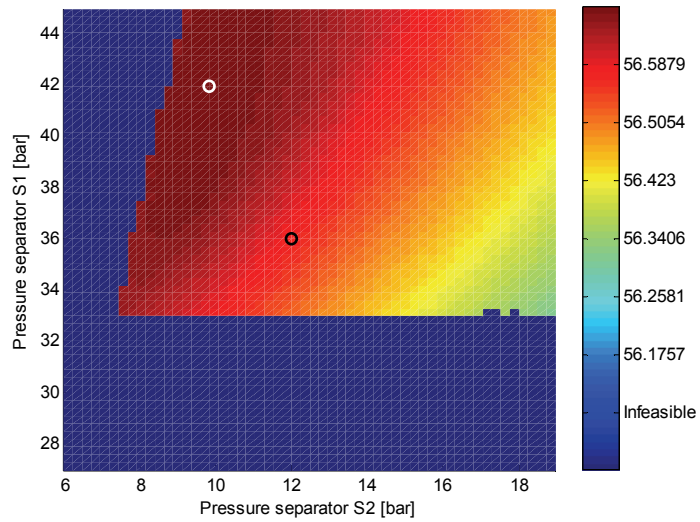


Figure 28: Profit as a function of the pressure in separator S1 and S2 for fluid 1.

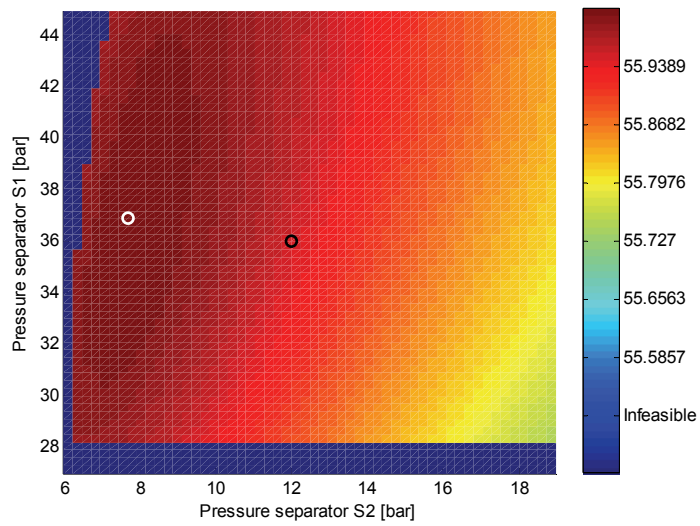


Figure 29: Profit as a function of the pressure in separator S1 and S2 for fluid 2.

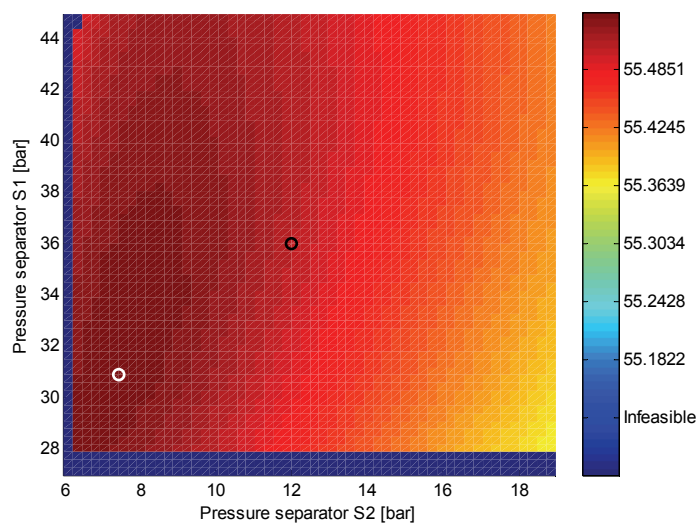


Figure 30: Profit as a function of the pressure in separator S1 and S2 for fluid 3.

The new control method increased the energy cost with 2.8 and 3.8 [%] for fluid 2 and 3, respectively. This is due to an increase in the gas turbine speed, see Table 10. For fluid 1 the energy cost was reduced with 0.5% for the new control method. This was expected since the pressure in separator S1 was increased and less compression was needed for the gas separated in this separator.

Table 10 shows that the gas valve opening for separator S1 and S2 are partially closed. This gives a large pressure drop over the valve. One example of this is the 2.5 bar pressure drop that occurs for experiment 1 with the new control method. Compressor C2 must therefore compress this gas 2.2 bar more than what is necessary if the valve was fully open. The two gas valve is not needed if the speed of two compressors can be selected independently. This will reduce the energy cost since this method does not require a pressure drop over the gas valves to control the pressure in the separators.

The new control method increased the profit with 0.17, 0.11 and 0.07[%] for experiment 1, 2 and 3, respectively. By assuming that the plant is operated in experiment 1, 2 and 3 for equal time shares a rough estimation of the increase in profit can be calculated. This rough estimation gives an increase in profit of two million dollars per year.

The profit is equal to the income for the optimization of separator pressure without compressor, see Section 5. As expected the percentage increase in profit is lower when the compressors are included into the model. This is because the compressors reduce the feasible region and that the new set-points give an increase in the energy cost.

Table 9: Comparison of profit between old and new control method.

	Fluid 1		Fluid 2		Fluid 3	
	Old [\$/s]	New [\$/s]	Old [\$/s]	New [\$/s]	Old [\$/s]	New [\$/s]
<b>Income</b>	56.92	57.02	56.28	56.21	55.77	55.82
<b>-Expense</b>	0.3503	0.3483	0.2591	0.2664	0.2603	0.2703
<b>=Profit</b>	56.57	56.67	56.01	55.95	55.51	55.55

Table 10: Output data and setpoints for the old and new control method.

	Fluid 1		Fluid 2		Fluid 3	
	Old	New	Old	New	Old	New
<b>U<sub>1</sub></b>	0,9043	0,2653	0,3999	0,09872	0,1723	0,2632
<b>U<sub>2</sub></b>	0,1907	0,9229	0,1892	0,9448	0,1548	0,8485
<b>P<sub>d,C2</sub> [bar]</b>	148,6	148,0	148,0	148,2	148,0	148,063
<b>P<sub>1</sub> [bar]</b>	36	42	36	36.9	36	30.9
<b>P<sub>2</sub> [bar]</b>	12	9.84	12	7.68	12	7.44
<b>S</b>	1.0005	0.996	0.94575	0.9983	0.94575	1.002
<b>P<sub>r,C4</sub> [bar]</b>	4.4	4.76	5	3.76	5	3.68

The current control system gives an infeasible operation point for fluid 4, see Figure 31. This will activate the secondary pressure control system and some of the gas will be burned at the torch.

With the current control system the operator has two options:

1) Reduce the opening of the valve placed between the reservoir and the first stage separator. This will reduce the production rate and the operation point will again be feasible. The drawback with this method is that less crude oil is produced and this leads to a reduction in income. The maximum inlet flow for fluid 4 with the current control system is 12750 [kmol/h] and this gives a profit of 51.92 dollar per second.

2) Let some of the gas be burned at the torch. This gives atmospheric emission and taxes must be paid for this. Future income is also reduced since less gas is injected back to the reservoir. The simulation model must be extended to also include the safety pressure system, gas price and taxes on emissions for a compression between method two and the new control system can be done. This is out of scope for this thesis.

With the new control system, operation under this condition is feasible and the maximum capacity for the gas oil separation plant is therefore extended. The new control system increased the profit with 11% for this operation point.

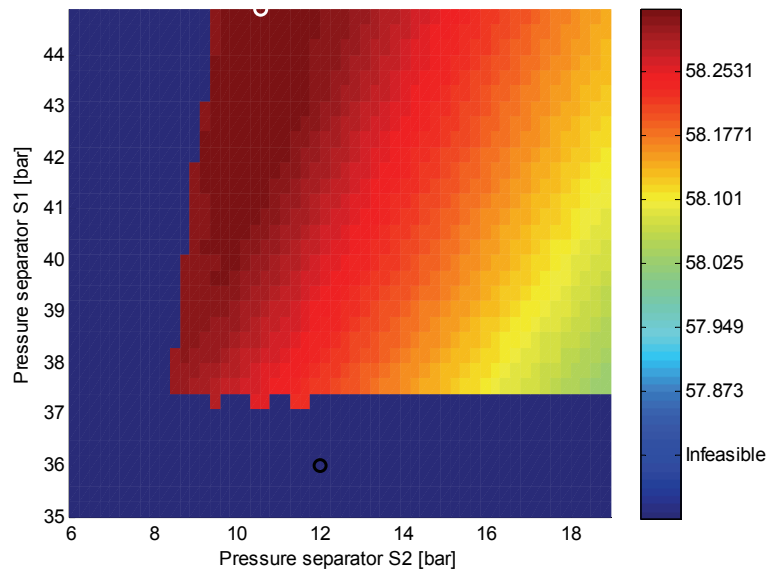


Figure 31: Profit as a function of the pressure in separator S1 and S2 for fluid 4.





## 9 Conclusions

In this thesis a steady state model of a multistage crude oil production plant with compressors has been implemented in MATLAB. This model has been used to investigate the potential benefits of using adaptive separator pressure.

First, a gas oil separation plant with two stages was used to show that the oil recovery was dependent on the separator pressure and the reservoir fluid composition. This example demonstrated that adaptive separator pressure could increase oil recovery and income from crude oil sale.

Then, a literature study on separator modelling was performed and a vapour liquid equilibrium calculation was chosen to model the separators. This model used the Peng Robinson equation of state and successive substitution. The vapour liquid equilibrium calculation was implemented in MATLAB and tested against a commercial process simulator. Both simulators gave almost identical result for a test case, which consists of a three stage gas oil separation plant. The average relative error in the mass flows and equilibrium values was 0.13%.

Dimensionless parameters method was used to model the centrifugal compressors since it was easy to implement and accurate for off-design operation. Polynomial approximation and physical modelling were also investigated, but these two methods were found to be unsuitable for this type of modelling.

A steady state simulation model of a multistage crude oil production plant with gas compression was implemented in MATLAB. Brute force optimization was used to maximize the profit by changing the separator pressure. Three different inlet conditions were tested and the profit was increased with 0.17, 0.11 and 0.07 percent compared to the old control method. A rough estimation shows that the new control method can increase the profit with two million dollars per year for Snorre A.

The new control method has a large maximum capacity for inlet flow with high gas oil ratio. A simulation showed that the new control method could increase profit with 11 percent for this inlet condition.



## 10 Appendix

### 10.1 Linear least-squares problem

The coefficients for a polynomial with one independent variable can easily be found by using the MATLAB command *polyfit*. This function cannot be used for polynomials with more than one independent variable. In Equation (10.2) a polynomial with two independent variables is presented. This section will present a method that calculates the coefficients for this polynomial.

For a system with  $l$  data points, see Equation(10.1), a function  $f(x,y)$  can be determined such that  $f(x_i, y_i) \approx z_i, i=1, \dots, l$ . The function  $f(x,y)$  is a polynomial and this polynomial is presented in Equation (10.2). Here,  $c_{1,1}$  to  $c_{n+1,m+1}$  are the unknown coefficients.

$$(z_1, x_1, y_1), \dots, (z_l, x_l, y_l) \quad (10.1)$$

$$\begin{aligned} f(x_j, y_j) &= c_1 x_j^n + c_2 x_j^{n-1} + \dots + c_n x_j + c_{n+1} \\ c_1 &= c_{1,1} y_j^m + c_{1,2} y_j^{m-1} + \dots + c_{1,m} y_j + c_{1,m+1} \\ &\vdots \\ c_{n+1} &= c_{n+1,1} y_j^m + c_{n+1,2} y_j^{m-1} + \dots + c_{n+1,m} y_j + c_{n+1,m+1} \end{aligned} \quad (10.2)$$

Equation (10.2) can be rearranged to Equation(10.3). To simplify the notation subscript  $j$  is omitted in Equation(10.3).

$$\begin{aligned} f(x, y) &= A\theta^T \\ A &= \begin{bmatrix} y^m x^n & y^{m-1} x^n & \dots & 1x^n & y^m x^{n-1} & y^{m-1} x^{n-1} & \dots & 1x^{n-1} & \dots & y^m 1 & y^{m-1} 1 & \dots & 1 \end{bmatrix} \\ \theta &= \begin{bmatrix} c_{1,1} & c_{1,2} & \dots & c_{1,m+1} & c_{2,1} & c_{2,2} & \dots & c_{2,m+1} & \dots & c_{n+1,1} & c_{n+1,2} & \dots & c_{n+1,m+1} \end{bmatrix} \end{aligned} \quad (10.3)$$

$$z_j = A_j \theta^T \quad \text{for}(j=1, 2 \dots l) \quad (10.4)$$

$$\begin{bmatrix} A_1 \\ A_2 \\ \vdots \\ A_l \end{bmatrix} \quad (10.5)$$

The system in Equation (10.4) consists of  $l$  linear equations in  $(n+1)(m+1)$  unknown coefficients. To get a unique solution two conditions must be satisfied. The number of linear equations must be larger than the number of unknown coefficients and matrix (10.5) must have full column rank.

Usually it is impossible to find a  $\theta$  that satisfied Equation (10.4) for all linear equations. A linear least-squares problem can be formulated to minimize the error, see Equation(10.6). The problem is convex and this ensures that the solution found is the global minimum. For theory and solution methods for linear least-squares problem consult (Nocedal & Wright, 2006).

$$\min_{\theta} \sum_{j=1}^n (z_j - A_j \theta^T)^2 \quad (10.6)$$

In MATLAB the least-squares solution is obtained by using the ‘backslash’ operator as seen in Equation (10.7).

$$\theta = \begin{bmatrix} A_1 \\ A_2 \\ \vdots \\ A_l \end{bmatrix} \backslash \begin{bmatrix} z_1 \\ z_2 \\ \vdots \\ z_l \end{bmatrix} \quad (10.7)$$

## ***10.2 Reservoir fluid composition***

The exact reservoir fluid composition was not possible to obtain and is therefore estimated. In this estimation the design gas composition for compressor C1 and a C7+ fraction is used. All hydrocarbons with more than seven carbon molecules are placed in the C7+ fraction. The most important factor in the reservoir fluid is the gas oil ratio. Three different reservoir fluids, fluid 1 to 3, are made. The C7+ fraction (oil) for these fluids are 15, 30 and 45 mole present, respectively.

Table 13 presents the gas analysis for compressor C1 and is collected from Aker Engineering a.s, (1996a). In this analysis, small traces of the polar components: Water vapour, Carbon Dioxide and Hydrogen Sulphide are present. The vapour liquid algorithm implemented in MATLAB does not support polar components and these components must therefore be set to zero. These three components account for approximately 0.5 mol % of the total gas composition and should therefore be safe to remove.

Table 11: Gas analysis for compressor C1.

Component	Composition [Mol %]
Nitrogen	2.425
Water Vapour	0.021
Carbon Dioxide	0.472
Hydrogen Sulphide	0.007
Methane	69.740
Ethane	13.345
Propane	9.347
i-Butane	0.918
n-Butane	2.567
i-Pentane	0.420
n-Pentane	0.483
Hexane Plus	0.256

Table 14 shows the reservoir fluid composition. The composition is normalized such that the C7+ fraction and the components from Table 11 together give a composition of 100 mol percent.

Table 12: Reservoir fluid composition.

Component	Composition [Mol %]			
	Fluid 1	Fluid 2	Fluid 3	Fluid 4
Nitrogen	2.071	1.706	1.341	1.832
Methane	59.58	49.06	38.55	61.87
Ethane	11.40	9.390	7.377	12.74
Propane	7.984	6.577	5.167	7.053
i-Butane	0.784	0.646	0.507	0.693
n-Butane	2.193	1.806	1.419	1.940
i-Pentane	0.358	0.295	0.232	0.316
n-Pentane	0.412	0.340	0.266	0.364
n-Hexane	0.218	0.180	0.141	0.192
C7+	15.00	30.00	45.00	13.00

### 10.3 Chemical properties

The chemical properties needed in this project are: the critical temperature, the critical pressure, the acentric factor and molecular weight. The chemical properties used in this project are collected from Yaws (1999) and is presented in Table 13.

The C7+ fraction uses the critical temperature, critical pressure and acentric factor from n-hexadecane. The molecule weight for the C7+ fraction is set to 295 [g/mol]. The molecule weight from n-hexadecane gave a too high API number and is therefore not used. A more accurate method to determine the chemical properties for the C7+ fraction is to use experimental data. Twu (1984) proposed a method for estimating the critical properties and molecular weight of the C7+ fraction.

Table 13: Chemical properties.

Component	critical temperature [K]	critical pressure [Pa]	acentric factor	molecular weight [g/mol]
Nitrogen	126.10	33.94e5	0.040	28.013
Methane	190.58	46.04e5	0.011	16.043
Ethane	305.42	48.8 e5	0.099	30.070
Propane	369.82	42.49 e5	0.152	44.096
i-Butane	408.14	36.48 e5	0.177	58.123
n-Butane	425.18	37.39 e5	0.199	58.123
i-Pentane	460.43	33.81 e5	0.228	72.150
n-Pentane	469.65	33.69 e5	0.249	72.150
n-Hexane	507.43	30.12 e5	0.305	86.177
C7+	702.60	14.19 e5	0.747	295.00

### 10.4 Inlet condition for the compressor characteristics

This thesis uses a surge avoidance controller and the compressor system will therefore always operate in the stable part. This part of the compressor characteristics is obtained by direct measurements since it is experimentally observable (Wang & Murray, 1998). In Table 14 the inlet conditions for this experiment are presented.

Table 14: Inlet conditions for the compressor characteristics.

	Temperature [°C]	Molecular weight [gram/mol]	Pressure [Bar]
Compressor C2	29.8	22.831	34.25
Compressor C3	29.7	29.316	10.8
Compressor C4	28.6	42.756	1.3

## 10.5 Simple PI control with anti-windup

The PI controller used in this project is the PI controller from Hovd (2008). The anti windup limits the controller output and the controller is implemented as illustrated in Figure 32. Here  $E$  is the error,  $K_p$  is the proportional gain,  $T_i$  is the integral gain,  $s$  is the Laplace operator,  $u$  is the valve opening,  $u_{\max}$  is the maximum valve opening and  $u_{\min}$  is the minimum valve opening.

According to Hovd (2008), The actual input implemented on the plant is feedback to the controller through the low pass filter  $1/(T_i s + 1)$ . If the actual plant input is not measured, it suffices to know the range of actuation for the input. The actual input can then easily be calculated.

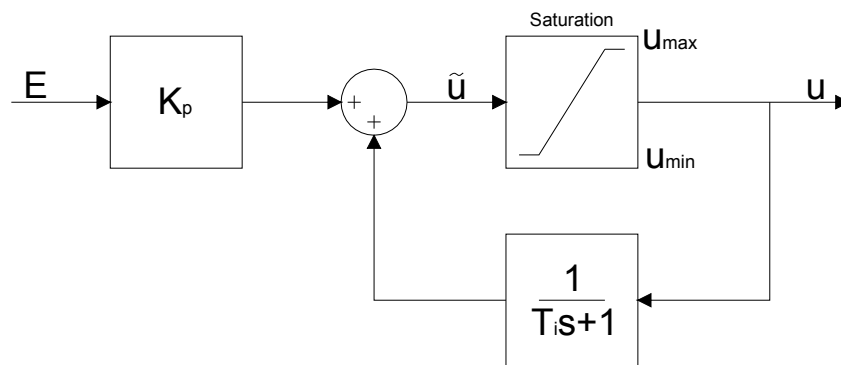


Figure 32: PI controller with anti-windup.

The normal behaviour of a PI controller is achieved when the valve opening is not saturated ( $\tilde{u} = u$ ), see Equation (10.8).

$$u = K_p \frac{T_i s + 1}{T_i s} E \quad (10.8)$$

It is assumed that the capacity of the recycle valve is large and that  $\tilde{u}$  is smaller than  $u_{\max}$  for all steady state operation points. Equation (10.9) presents the controller behaviour when it is saturated at the lower limit. The internal feedback path in the controller is now broken and integrating state does not wind up.

$$\tilde{u} = K_p E + \frac{1}{T_i s + 1} u_{\min} \quad (10.9)$$

A positive error will lead to an increase in the valve opening. This will reduce system friction and the mass flow through the compressor will therefore increase. An increase in mass flow will decrease the positive error, see Equation (7.21). The steady state error must therefore be equal or less than zero.

## 10.6 Pseudocode for brute force optimization of a gas oil separation plant

```
 $p_{s1} = [27 \quad 27.3 \quad \dots \quad 45]$   
 $p_{s2} = [6 \quad 6.24 \quad \dots \quad 19]$   
 $S = [0.9 \quad 0.90075 \quad \dots \quad 1.05]$   
 $p_{r,C4} = [3 \quad 3.04 \quad \dots \quad 9]$   
 $P_{opt} = 0$   
for  $j = 1 : \text{size}(p_{s1})$   
  for  $k = 1 : \text{size}(p_{s2})$   
    compute separator model and  $I = f(p_{s1}(j), p_{s2}(k))$   
    for  $l = 1 : \text{size}(S)$   
      for  $m = 1 : \text{size}(p_{r,C4})$   
        compute compressor model and  $E = f(p_{s1}(j), p_{s2}(k), S(l), p_{r,C4}(m))$   
         $P = I - E$   
        if (feasible region and  $P > P_{opt}$ )  
           $P_{opt} = P \quad j_{opt} = j \quad k_{opt} = k \quad l_{opt} = l \quad m_{opt} = m$   
        end  
      end  
    end  
  end  
end  
end  
end  
end
```



## 10.7 Enclosed files

The simulation models and the MATLAB code are easier to study in MATAB than as an attachment in this report. Table 15 shows a listing of the contents on the enclosed files.

Table 15: Contents on the enclosed files.

Folder	File	Description
Antisurgecontroller	CompressorC23.m	Generates the plot presented in Figure 26.
Bobbeldew	BubbeldewCri.m	Generates the plot presented in Figure 6.
	BubbleDew	Contains the data from UNISIM.
Comchar	comcharC2.m comcharC3.m comcharC4.m	Generates the compressors characteristics from the manufacture for compressor C2, C3 and C4
Commod	CompressorC4.m	Generates the plot presented in Figure 27.
Commod\dim	Dimpar.m	Calculates the unknown coefficients for the dimensionless parameters model.
	objcch2.m	Implementation of the algorithm presented in Section 7.3.1.
	comcharC32.m	Extended version of the compressor characteristics for compressor C3
	PrecC2.fig PrecC3.fig PowC2.fig PowC3.fig	Figures generated by Dimpar.m.
	Plotdimpar.m	Generates the plot presented in Figure 23.
	Testsscompresor.m	Generates the plot presented in Figure 24
	sscomdim1.m	Steady state compressor model for compressor C2 and C3. This model uses dimensionless parameters and anti surge control is not included in this model.
	Sscomdim2.m	Same as sscomdim1.m, but with anti surge control
Commod\poly\C2	PRpoly1.m	Generates the plot presented in Figure 19.
	PRpoly2.m	Generates the plot presented in Figure 20.
	PRpolynon.m	Generates the plot presented in Figure 21.
	objf9.m	Subroutine called by PRpolynon.m.
	Popolynon.m	Generates the plot presented in Figure 22.
	Obj13.m	Subroutine called by Popolynon.m.
Commod\poly\C3		Generates the plot presented in Figure 19 to Figure 22 for compressor C3. Not included in the report.
Empirical method	plotrap.m	Generates the plot presented in Figure 3.
Isentropic efficiency	iseC2.m	Generates the plot presented in Figure 17.

VLE	API.m	Calculates the API gravity of crude oil, se Section 4.6.
	flashcalc.m	Isothermal flash calculation using Peng Robinson equation of state, se Section 4.4.
	oilrecovery.m	Generates the plot presented in Figure 2.
	Opi1.m	Optimizes the separator pressure for a process without compressors, see Section 5
	Phi.m	Fugacity coefficient calculation using Peng Robinson equation of state
	Verify.m	Compares the MATLAB implementation of the vapour liquid equilibrium calculation against a commercial simulator, see Section 4.5.
VLEandComp	bruteopti.m	Optimizes the separator pressure for a process with compressors, see Section 0
	compressors.m	Contains the compression model.
	Separators.m	Contanis the separator model.
	maxflow.m	Calculates the maximum possible flow for fluid 4 and oil and gas production
	sscompressorC4.m	Steady state compressor model for compressor C4, see Section 7.5

## 10.8 Acronyms

Table 16: Acronyms.

CPS	Chemical process simulators
EOS	Equation of state
MPC	Model Predictive Control
MSc	Master of Science
NOK	Norwegian krone
OPC	Object Linking and Embedding for Process Control
PR	Peng Robinson
RK	Redlich Kwong
RTO	Real Time Optimization
SS	Successive substitution
VLE	Vapour liquid equilibrium

## 11 Bibliography

Abdel-Aal, H., M Aggour & M.A. Fahim (2003). *Petroleum and gas field processing*. Marcel dekker, inc.

Adewumi, M. (n.d.). *Phase Relations in Reservoir engineering*. Retrieved from The Pennsylvania State University: <https://www.e-education.psu.edu/png520/>

Adjiman, C., Dallwig, S., Floudas, C., & Neumaier, A. (1997). *A global optimization method, alfaBB, for general twice-differentiable constrained NLPs -- I. Theoretical advances*. Computers & Chemical Engineering.

Ahmed, T. H. (2006). *Reservoir engineering handbook*. Elsevier Inc.

Aker Engineering a.s. (1995b). *2nd Stage Separator Data Sheet Process and Mechanical*.

Aker Engineering a.s. (1996a). *Mechanical data sheet for gas compression train. Vigdis field development project*.

Arnold, K., & Stewart, M. (1999). *Surface Production Operations (2nd Edition) Volume 1 - Design of Oil-Handling Systems and Facilities*. Elsevier.

Assael, M. J., Trusler, M. J., & Tsolakis, T. F. (1996). *Thermophysical properties of fluids : an introduction to their prediction*. London: Imperial College Press.

Bahadori, A., Vuthaluru, H. B., & Mokhatab, S. (2008). *Optimizing separator pressures in the multistage crude oil production unit*. Asia-pacific journal of chemical engineering.

Bøhagen, B. (2007). *Active surge control of centrifugal compression systems*.

Carroll, J. (2003). *Natural Gas Hydrates - A Guide for Engineers*. Elsevier.

Casavant, T. E., & Côté, R. P. (2004). *Using chemical process simulation to design industrial ecosystems*. Journal of Cleaner Production.

Chaikunchuensakun, S., Stiel, L. I., & Baker, E. L. (2002). *A Combined Algorithm for Stability and Phase Equilibrium*. Industrial & Engineering Chemistry Research.

Clark, N. (1960). *Elements of Petroleum Reservoirs*. Dallas: Society of Petroleum Engineers.

Cohen, H. C., Saravanamuttoo, H., & Rogers, G. (1996). *Gas Turbine Theory*. Longman. Essex.

Croft, A., Davison, R., & Hargreaves, M. (2001). *Engineering Mathematics: A Foundation for Electronic, Electrical, Communications and Systems Engineers*. Pearson Education Limited.

Danesh, A. (1998). *PVT and Phase Behaviour of Petroleum Reservoir Fluids*. Elsevier.

- Devold, H. (2006). *Oil and gas production handbook: An introduction to oil and gas production*. ABB.
- Dixon, S., & Eng, B. (1998). *Fluid Mechanics, Thermodynamics of Turbomachinery*. Elsevier.
- E24 AS. (n.d.). *E24*. Retrieved from <http://e24.no>
- Egeland, O., & Gravdahl, J. (2002). *Modeling and simulation for control*. Trondheim: Marine Cybernetics.
- Firoozabadi, A. (1999). *Thermodynamics of hydrocarbon reservoirs*. McGraw-Hill.
- Forsthoffer, W.E. (2005) *Forsthoffer's Rotating Equipment Handbooks*. Elsevier.
- Ghosh, P. (1999). *Prediction of Vapor-Liquid Equilibria Using Peng-Robinson and Soave-Redlich-Kwong Equations of State*. Chemical Engineering & Technology.
- Gravdahl, J. T., & Egeland, O. (1999). *Compressor Surge and Rotating Stall*. London: Springer Verlag.
- Hanlon, P. (2001). *Compressor Handbook*. McGraw-Hill.
- Harding, S., & Floudas, C. (1999). *Phase Stability with Cubic Equations of State: A Global Optimization Approach*.
- Hauger, S. O. (2008). *MPC Model Predictive Control*.
- Helvoirt, J. v. (2007). *Centrifugal Compressor Surge Modeling and Identification for Control*.
- Honeywell. (2008). *UniSim Design User Guides, References and Tutorials*.
- Hovd, M. (2008). *Lecture notes for the course Advance Control of Industrial Processes*. Norwegian university of science and technology.
- Ismail, I., Gamio, J., Bukharia, S., & Yang, W. (2005). *Tomography for multi-phase flow measurement in the oil industry*. Flow measurement and instrumentation.
- Jaluria, Y. (2008). *Design and optimization of thermal systems*. CRC Press.
- Lipták, B. G. (1995). *Instruments engineers's handbook: Process control*.
- Mehra, R. K., Heidemann, R. A., & Aziz, K. (1982). *Computation of multiphase equilibrium for compositional simulation*. Society of Petroleum Engineers journal.
- Mian, M.A. (2002). *Project Economics and Decision Analysis Volume I: Deterministic Models*. PennWell.

- Michelsen, M. L. (1982). *The isothermal flash problem. Part II. Phase-split calculation*. Fluid Phase Equilibria.
- Nichita, D. V., Broseta, D., & Hemptinne, J.-C. d. (2006). *Multiphase equilibrium calculation using reduced variables*. Fluid Phase Equilibria.
- Nichita, D. V., Gomez, S., & Luna, E. (2002). *Multiphase equilibria calculation by direct minimization of Gibbs free*. Computers and Chemical Engineering.
- Nocedal, J., & Wright, S. J. (2006). *Numerical Optimization*. Springer.
- Norsk Hydro. (2001). *Systemkurs Snorre og Vigdis*.
- Nørstebø, V. S. (2008). *Optimum operation of gas export systems*. Trondheim.
- O'Connell, J., & Haile, J. (2005). *Thermodynamics : fundamentals for applications*. Cambridge University Press.
- Peng, D.-Y., & Robinson, D. B. (1976). *A New Two-Constant Equation of State*. Industrial & Engineering Chemistry Fundamentals.
- Philip, T. J. (1999). *Simulation of Industrial Processes for Control Engineers*. Elsevier.
- Privat, R., Jaubert, J.-N., & Mutelet, F. (2008). *Addition of the sulfhydryl group (-SH) to the PPR78 model (predictive 1978)*. The Journal of Chemical Thermodynamics.
- Purdue research foundation. (2006). *Thermodynamic systems operating with near-isothermal compression and expansion cycles*.
- Rachford, H., & Rice, J. (1952). *Procedure for Use of Electronic Digital Computers in Calculating Flash Vaporization Hydrocarbon*.
- Rand, S. (2003). *Significance of Tests for Petroleum Products*. ASTM International.
- Rosales-Quintero, A. (n.d.). *Isothermal flash calculation using Soave equation of state*. Retrieved from MATLAB Central:  
<http://www.mathworks.com/matlabcentral/fileexchange/22364>
- Rossi, C., Cardozo-Filho, L., & Guirardello, R. (2009). *Gibbs free energy next term minimization for the calculation of chemical and phase equilibrium using linear programming*. Fluid Phase Equilibria.
- Saber, N., & Shaw, M. (2007). *Rapid and robust phase behaviour stability analysis using global optimization*. Fluid Phase Equilibria.
- Siemens. (1996). *Snorre/Vigdis Gas Antisurge Controller. Vigdis field development project*.

Twu, C. H. (1984). *An internally consistent correlation for predicting the critical properties and molecular weights of petroleum and coal-tar liquids*. Fluid Phase Equilibria.

Vázquez-Román, R., García-Sánchez, F., Salas-Padrón, A., Hernández-Garduza, O., & Eliosa-Jiménez, G. (2000). *An efficient flash procedure using cubic equations of state*. Chemical Engineering Journal.

Wang, Y., & Murray, R. M. (1998). *Effects of the Shape of Compressor Characteristics on Actuator*.

Wauquier, J.-P. (2000). *Petroleum refining Volume two*.

Whinery, K. F. Compbell, J. M. (1958). *Method for determining optimum second stage pressure in 3-stage separation*. J. of Petrol. Technol. 4.

White, F. M. (2008). *Fluid Mechanics*. McGraw-Hill.

Willems, F. (2000). *Modeling and Bounded Feedback Stabilization of Centrifugal Compressor Surge*.

Yaws, C.L. (1999). *Chemical Properties Handbook*. McGraw-Hill.

Zhu, Y., Wen, H., & Xu, Z. (2000). *Global stability analysis and phase equilibrium calculations at high pressures using the enhanced simulated annealing algorithm*. Chemical Engineering Science.